

Spike-Frequency Adapting Neural Ensembles: Beyond Mean Adaptation and Renewal Theories

Eilif Muller

emueller@kip.uni-heidelberg.de

Lars Buesing

lbuesing@kip.uni-heidelberg.de

Johannes Schemmel

schemmel@kip.uni-heidelberg.de

Karlheinz Meier

meierk@kip.uni-heidelberg.de

Kirchhoff Institute for Physics, University of Heidelberg, 69120 Heidelberg, Germany

We propose a Markov process model for spike-frequency adapting neural ensembles that synthesizes existing mean-adaptation approaches, population density methods, and inhomogeneous renewal theory, resulting in a unified and tractable framework that goes beyond renewal and mean-adaptation theories by accounting for correlations between subsequent interspike intervals. A method for efficiently generating inhomogeneous realizations of the proposed Markov process is given, numerical methods for solving the population equation are presented, and an expression for the first-order interspike interval correlation is derived. Further, we show that the full five-dimensional master equation for a conductance-based integrate-and-fire neuron with spike-frequency adaptation and a relative refractory mechanism driven by Poisson spike trains can be reduced to a two-dimensional generalization of the proposed Markov process by an adiabatic elimination of fast variables. For static and dynamic stimulation, negative serial interspike interval correlations and transient population responses, respectively, of Monte Carlo simulations of the full five-dimensional system can be accurately described by the proposed two-dimensional Markov process.

1 Introduction

Spike-frequency adaptation (SFA) refers to the intrinsic property of certain neurons to fire with gradually increasing interspike intervals (ISIs) in response to a steady injection of suprathreshold current. SFA is ubiquitous: It has been observed in many neural systems of diverse species (Fuhrmann, Markram, & Tsodyks, 2002). In the mammalian visual system, for example, the majority of retinal ganglion cells (RGCs) (O'Brien, Isayama, Richardson, & Berson, 2002), geniculate relay neurons (Smith, Cox, Sherman, & Rinzel,

2001), and neocortical and hippocampal regular spiking pyramidal neurons (McCormick, Connors, Lighthall, & Prince, 1985) exhibit SFA.

The in-vitro conditions used to experimentally verify the presence of SFA are far from the operational mode of a typical neuron in a network. Given cortical neuron firing rates and interconnectivity, each neuron there is under intense bombardment by both excitatory and inhibitory synapses. These mutually opposing showers of excitation and inhibition induce highly irregular fluctuations of the membrane potential reminiscent of a random walk. The resulting dominance of the mean synaptic conductances over the leak results in a markedly shortened effective membrane time constant, a dynamical regime known as the high-conductance state (Destexhe, Rudolph, & Paré, 2003; Shelley, McLaughlin, Shapley, & Wielaard, 2002). In this regime, action potentials are emitted when the membrane potential chances across the firing threshold and the resulting ISIs appear stochastic and are, for adapting neurons, roughly gamma distributed (Softky & Koch, 1993; Destexhe, Rudolph, Fellous, & Sejnowski, 2001; Dayan & Abbott, 2001).

Conductance-based phenomenological models for SFA and related relative refractory mechanisms are standard and given in Dayan and Abbott (2001) and Koch (1999) and recently generalized in Brette and Gerstner (2005). Benda and Herz (2003) show that a large class of biophysical mechanisms that induce SFA can be reduced to these conductance-based phenomenological models. Similar but current-based adaptation mechanisms have been studied in van Vreeswijk and Hansel (2001) and the related threshold fatigue model for adaptation, also known as dynamic threshold, in Chacron, Pakdaman, and Longtin (2003) and Lindner and Longtin (2003). See Ermentrout, Pascal, and Gutkin (2001) for a bifurcation analysis of I_{ahp} , the afterhyperpolarization current, a calcium-dependent potassium current, and I_{m} , the muscarinic slow voltage-dependent potassium current, two biophysical mechanisms behind SFA.

Mean-adaptation approximations for the firing rate of populations of spike-frequency adapting neurons augmenting the standard Wilson and Cowan equations (Wilson & Cowan, 1972) were devised in Latham, Richmond, Nelson, and Nirenberg (2000) and Fuhrmann et al. (2002) and used to study the synchronizing effects of SFA. Universal mean-adaptation methods for modeling the firing rate of adapting neurons subject to suprathreshold noise-free current input are given in Benda and Herz (2003). In La Camera, Rauch, Lüscher, Senn, and Fusi (2004), mean-adaptation methods are investigated to describe the static and dynamic firing rates of a large class of integrate-and-fire neuron models with current-based and dynamic threshold adaptation mechanisms driven by noisy input currents. The phenomenological firing rate relaxation dynamics of previous Wilson and Cowan studies is replaced in La Camera et al. (2004) with a firing rate that depends instantaneously on filtered synaptic currents, as suggested in Fourcaud and Brunel (2002) and Renart, Brunel, and Wang (2004). While

for the Wilson and Cowan approaches, the relaxation time constant is a free parameter, the approach due to La Camera et al. (2004) has no free parameters, and excellent agreement is reported in the static and dynamic case for several neuron models.

Originally introduced in Knight (1972) and recently the subject of intense study, population density formalisms provide powerful tools to understand neural ensemble and network behavior in a quantitative way (Brunel, 2000; Omurtag, Knight, & Sirovich, 2000; Nykamp & Tranchina, 2000, 2001; Fourcaud & Brunel, 2002; Meffin, Burkitt, & Grayden, 2004; Renart et al., 2004). Such studies are mostly restricted to exactly solvable white noise input cases, with notable exceptions (Nykamp & Tranchina, 2001; Fourcaud & Brunel, 2002). In Fourcaud and Brunel (2002), the key observation is made that colored input noise due to synaptic filtering results in a nonzero probability density near threshold and allows neurons to respond instantaneously to injected currents. This provides the theoretical basis for studies such as La Camera et al. (2004) and will also play an important role in the work here. Conductance-based neurons with finite synaptic time constants are treated in Rudolph and Destexhe (2003a, 2005), Richardson (2004), Richardson and Gerstner (2005), though only in the subthreshold regime, limiting their applicability for understanding firing rate, and networks dynamics. The problem with threshold has yet to be solved exactly, however, it is treated in Moreno-Bote and Parga (2004, 2005).

For neurons without SFA driven by noisy input, an alternate and fruitful approach is to apply renewal theory as presented in detail in Gerstner and Kistler (2002). With the defining characteristic of renewal theory being that successive ISIs are statistically independent, these models neglect by definition the observation in Chacron et al. (2003) and Lindner and Longtin (2003) that SFA induces negative serial ISI correlations.

While the great majority of excitatory neurons exhibit SFA, there has yet to be a population density treatment accounting for it, given the difficulty in treating the added dimension analytically and numerically. We present here a study whereby the ensemble behavior of adapting neurons in the high-conductance state can be understood in a quantitative way.

We start by considering in section 2 how to go beyond the renewal theory formalism of Gerstner and Kistler (2002) by introducing a dependence between ISIs, resulting in a Markov model described by a master equation. A connection to renewal theory is found by a suitable variable transformation, and expressions for the ISI distribution and conditional ISI distribution are derived. We then consider in section 3 the full five-dimensional master equation of the canonical conductance-based integrate-and-fire neuron model driven by Poisson spike trains augmented by SFA and a relative refractory mechanism of the form given in Dayan and Abbott (2001). By applying an adiabatic elimination of fast relaxing variables (Haken, 1983; Gardiner, 1984), we argue that this five-dimensional master equation can be approximated by a two-dimensional master equation of the same form as the

“beyond renewal theory” Markov model proposed in section 2. In section 4, we determine the generalized hazard function required for the Markov model by fitting to Monte Carlo simulations of the full system, given that the firing rate of the neuron model we employ has yet to be solved exactly. By reasoning as in Fourcaud and Brunel (2002), Renart et al. (2004), and La Camera et al. (2004), we show how the generalized hazard function applies in the dynamic case by accounting for synaptic filtering. In section 5, we provide numerical methods for solving the master equations and generating realizations of the proposed Markov processes. In section 6, predictions for ISI correlations and conditional ISI distributions in the static case, and firing rates in the dynamic case due to the proposed Markov model are compared to Monte Carlo simulations of the full system. Finally in section 7, the master equation is employed to analyze the domain of validity of mean-adaptation approaches.

2 Beyond Renewal Theory

Gerstner and Kistler (2002) demonstrate that for spike response models (a generalization of integrate-and-fire neuron models), the statistical ensemble of a single neuron with noise can be described using methods of inhomogeneous renewal theory, as reviewed in appendix C.

The basic assumption of inhomogeneous renewal theory is that the state of the modeled system can be described by a single state variable, τ , the time since last renewal, or age of the system, and time t . The limiting probability density for the neuron to spike, or more generally, for the system to renew after surviving a time interval τ ,

$$\rho(\tau, t) = \lim_{\Delta t \rightarrow 0^+} \frac{\text{prob}\{\geq 0 \text{ renewals in } [t, t + \Delta t] \mid \tau\}}{\Delta t}, \quad (2.1)$$

also known as the hazard function (Cox, 1962), is a function of time, t , and age, τ .¹ Thus, subsequent interspike intervals (ISIs) are by definition independent and uncorrelated.

As Gerstner and Kistler (2002, pp. 245), stated, “A generalization of the [renewal] population equation to neuron models with [spike-frequency] adaptation is not straightforward since the [renewal] formalism assumes that only the last spike suffices. . . . A full treatment of adaptation would involve a density description in the high-dimensional space of the microscopic neuronal variables [as in] (Knight, 2000).”

In section 3 we provide a full treatment of the density description mentioned above. However, before we proceed, it is instructive to consider what

¹For our discussion of renewal processes, we follow the notation of Cox (1962) but use τ to denote age, t to denote time, and ρ instead of h to denote the hazard function, as in appendix C.

a model might look like that allows for a dependence between subsequent ISIs.

Consider the standard phenomenological model for spike-frequency adaptation (SFA) proposed in Dayan and Abbott (2001) where a given neuron model is augmented with a conductance $g_s(t)$ that makes the jump $g_s(t + dt) = g_s(t) + q_s$ when the neuron spikes at time t and is otherwise governed by

$$\frac{dg_s(t)}{dt} = -\frac{1}{\tau_s} g_s(t). \quad (2.2)$$

Now consider a neuron that has g_s as a state variable and a probability density to fire of the form

$$h_g(g_s, t) = \lim_{\Delta t \rightarrow 0^+} \frac{\text{prob}\{> 0 \text{ spikes in } [t, t + \Delta t] \mid g_s\}}{\Delta t}, \quad (2.3)$$

where g_s evolves in time by equation 2.2. This process is analogous to a renewal process, but now with a single state variable, g_s , which is not reset at each occurrence of a spike but slowly forgets with a timescale of τ_s due to equation 2.2. For a model of this form, it is possible for correlations to arise between subsequent ISIs. We refer to both the renewal hazard function, $\rho(\tau, t)$, and the $h_g(g_s, t)$ defined here as hazard functions, as they both represent a probability density of the system to spike.

It is straightforward to show that the ensemble of such neurons is governed by a master equation of the form

$$\begin{aligned} \frac{\partial}{\partial t} P(g_s, t) = & \frac{\partial}{\partial g_s} \left[\frac{g_s}{\tau_s} P(g_s, t) \right] \\ & + h_g(g_s - q_s, t) P(g_s - q_s, t) \\ & - h_g(g_s, t) P(g_s, t), \end{aligned} \quad (2.4)$$

where $P(g_s, t)$ is the distribution of state variables g_s with $P(g_s < 0, t) \equiv 0$. The distribution $P(g_s, t)$ is analogous to the distribution of ages, $f^-(\tau, t)$, of renewal theory, and equation 2.4 is analogous to the renewal theory equation C.7, both given in appendix C. The model defined by equation 2.4 is referred to as the 1D Markov (1DM) model throughout the text. (See Table 1 for an overview of the models considered in the text.)

Understanding the connection of the 1DM model to its renewal theory cousin is facilitated by transforming g_s to a pseudo-age variable t_s with $\frac{d}{dt}t_s = 1$ by²

$$t_s = \eta(g_s) := -\tau_s \log(g_s/q_s). \quad (2.5)$$

The hazard function $h_g(g_s, t)$ becomes $h(t_s, t) = h_g(\eta^{-1}(t_s), t)$, a hazard function as in equation 2.1 of the pseudovariable t_s but defined also for $t_s < 0$. The distribution of states $P(g_s, t)$ becomes $P(t_s, t)$, where they are related by

$$P(t_s, t) = P(g_s = \eta^{-1}(t_s), t) \frac{d}{dt_s} \eta^{-1}(t_s). \quad (2.6)$$

The reset condition is not $t_s \mapsto 0$ as for a renewal process, but $t_s \mapsto \eta(g_s + q_s)$, where the right-hand side can be expressed in terms of t_s using the relation $g_s = \eta^{-1}(t_s)$. Defining the reset mapping, $\psi(t_s)$, such that the reset condition becomes $t_s \mapsto \psi(t_s)$, it follows that

$$\begin{aligned} \psi(t_s) &= \eta(\eta^{-1}(t_s) + q_s) \\ &= -\tau_s \log\left(\exp\left(\frac{-t_s}{\tau_s}\right) + 1\right), \end{aligned} \quad (2.7)$$

with its inverse given by

$$\psi^{-1}(t_s) = -\tau_s \log\left(\exp\left(\frac{-t_s}{\tau_s}\right) - 1\right), \quad (2.8)$$

whereby $\psi(\psi^{-1}(t)) = t$ and $\psi^{-1}(\psi(t)) = t$ as required by the definition of the inverse.

The variable t_s is then a general state variable that no longer represents the time since the last spike, as in renewal theory. Since $\psi : \mathbb{R} \rightarrow \mathbb{R}^-$, it follows that all trajectories are reinserted at negative pseudo-ages, and it can be seen from the form of ψ that “younger” spiking trajectories are reinserted at more negative pseudo-ages. This dependence of the reinserted state on the state just prior to spiking yields a Markov process (Riskin, 1996), which cannot be described by renewal theory.

²We follow the convention throughout the text of using positional arguments for functions and labeled arguments for derivatives. Probability distributions are excepted from this rule, as they are not functions but densities. The notation “:=” denotes definition of a function and its positional arguments.

The master equation in terms of t_s takes the form

$$\begin{aligned} \frac{\partial}{\partial t} P(t_s, t) = & -\frac{\partial}{\partial t_s} P(t_s, t) \\ & + \begin{cases} -h(t_s, t)P(t_s, t), & t_s \geq 0 \\ h(\psi^{-1}(t_s), t)P(\psi^{-1}(t_s), t) - h(t_s, t)P(t_s, t) & t_s < 0, \end{cases} \end{aligned} \quad (2.9)$$

revealing the advantage of the variable transformation $g_s \rightarrow t_s$: The deterministic drift term in equation 2.4 for the exponential decay of g_s is transformed to a constant drift term in t_s analogous to age in renewal theory. As a result, much can be calculated by analogy to renewal theory, and we are freed from the difficulty of treating the nonconstant drift toward zero in equation 2.4 numerically. We will see in later sections that $h(t_s, t)$ is in practice approximately of the form

$$h(t_s, t) = a(t) \exp(-b(t)q_s \exp(-t_s/\tau_s)) \quad (2.10)$$

when modeling spike-frequency adapting neurons in the high-conductance state, where $a(t)$ and $b(t)$ are determined by the stimulus.

For the static case where $h(t_s, t) \equiv h(t_s)$, $P(t_s)$ can be found from equation 2.9 by setting $\partial/\partial t P(t_s, t) = 0$. The resulting equation for $t_s \geq 0$,

$$\frac{\partial}{\partial t_s} P(t_s) = -h(t_s)P(t_s), \quad (2.11)$$

is exactly as for a renewal process. The solution is the homogeneous survival function,

$$P(t_s) = k\mathcal{W}(t_s, 0), \quad (2.12)$$

where

$$k^{-1} = \int_{-\infty}^{\infty} \mathcal{W}(t_s, 0) dt_s \quad (2.13)$$

is a constant of normalization, and the survival function,

$$\mathcal{W}(\Delta t, t_s^0) = \exp\left(-\int_0^{\Delta t} h(t_s^0 + s) ds\right), \quad (2.14)$$

and analogously the inhomogeneous survival function,

$$\mathcal{W}(\Delta t, t_s^0, t) = \exp\left(-\int_0^{\Delta t} h(t_s^0 + s, t + s) ds\right), \quad (2.15)$$

represent the probability that a system with initial state $t_s^0 \in \mathbb{R}$ will survive for a time Δt , and a time Δt after t , respectively and are analogous to the survival function of renewal theory as discussed in appendix C, except for the explicit dependence on the initial state t_s^0 . For $t_s < 0$, we solve $P(t_s)$ numerically by discretizing and integrating back from $t_s = 0$.

The distribution of pseudo-ages just prior to spiking at t , $P^*(t_s, t)$, is related to $P(t_s, t)$ by

$$P^*(t_s, t) = \frac{h(t_s, t)P(t_s, t)}{\alpha(t)}, \quad (2.16)$$

where

$$\alpha(t) = \int_{-\infty}^{\infty} h(t_s, t)P(t_s, t)dt_s \quad (2.17)$$

is a normalizing constant and also the firing rate of the ensemble.

The distribution of pseudo-ages just after spiking at t , $P^\dagger(t_s, t)$, is related to $P^*(t_s, t)$ by transforming variables by the reset mapping (see equation 2.7) for a probability distribution:

$$P^\dagger(t_s, t) = P^*(\psi^{-1}(t_s), t) \frac{d}{dt_s} \psi^{-1}(t_s). \quad (2.18)$$

2.1 Computing Renewal Quantities. The various quantities of renewal theory such as the ISI distribution, hazard function, and survival function are of interest and are straightforward to calculate for the proposed Markov process.

First, the renewal survival function, $\mathcal{F}(\tau, t)$, the probability that a system that spiked at t will survive the time interval τ , is given by

$$\mathcal{F}(\tau, t) = \int_{-\infty}^{\infty} \mathcal{W}(\tau, t_s, t) P^\dagger(t_s, t) dt_s. \quad (2.19)$$

The ISI distribution, $f(\tau, t)$, the probability that a neuron that spiked at t will survive for an interval τ and subsequently spike at $t + \tau$, is

$$f(\tau, t) = \int_{-\infty}^{\infty} h(t_s + \tau, t + \tau) \mathcal{W}(\tau, t_s, t) P^\dagger(t_s, t) dt_s. \quad (2.20)$$

Equivalently in terms of $P^*(t_s, t)$,

$$f(\tau, t) = \int_{-\infty}^{\infty} h(\psi(t_s) + \tau, t + \tau) \mathcal{W}(\tau, \psi(t_s), t) P^*(t_s, t) dt_s. \tag{2.21}$$

The hazard function of the system in a renewal sense, $\rho(\tau, t)$, where τ is a true age, is by definition the firing rate of the subpopulation that previously spiked at time $t - \tau$. Thus,

$$\rho(\tau, t) = \int_{-\infty}^{\infty} h(t_s, t) P(t_s, t | \text{spike at } t - \tau) dt_s, \tag{2.22}$$

where the state distribution of the system given a spike at $t - \tau$, $P(t_s, t | \text{spike at } t - \tau)$, can be determined by reasoning that it is the distribution of states just after spiking with arguments $t_s - \tau$ and $t - \tau$, $P^\dagger(t_s - \tau, t - \tau)$, which subsequently survive the interval τ ,

$$P(t_s, t | \text{spike at } t - \tau) = k_1 \mathcal{W}(\tau, t_s - \tau, t - \tau) P^\dagger(t_s - \tau, t - \tau), \tag{2.23}$$

where k_1 is the normalization factor,

$$k_1^{-1} = \int_{-\infty}^{\infty} \mathcal{W}(\tau, t_s - \tau, t - \tau) P^\dagger(t_s - \tau, t - \tau) dt_s, \tag{2.24}$$

and by inspection of equation 2.19,

$$k_1^{-1} = \mathcal{F}(\tau, t - \tau), \tag{2.25}$$

such that

$$\rho(\tau, t) = \frac{1}{\mathcal{F}(\tau, t - \tau)} \int_{-\infty}^{\infty} h(t_s, t) \mathcal{W}(\tau, t_s - \tau, t - \tau) P^\dagger(t_s - \tau, t - \tau) dt_s. \tag{2.26}$$

Clearly, the numerator is just $f(\tau, t - \tau)$, resulting in

$$\rho(\tau, t) = \frac{f(\tau, t - \tau)}{\mathcal{F}(\tau, t - \tau)}. \tag{2.27}$$

This verifies that the standard renewal theory relation that $f(\tau) = \rho(\tau)\mathcal{F}(\tau)$, generalized for the inhomogeneous case, still holds even though the underlying stochastic process is not a renewal process. It is interesting to note that in the inhomogeneous case, there is an alternate definition for the ISI distribution that is equally sensible: define $\hat{f}(\tau, t)$ as the probability that

a neuron that spiked at $t - \tau$ will survive the interval τ and subsequently spike at t . This is the ISI distribution that treats the spike at t as the final spike of the ISI rather than the initial spike as in equation 2.21. If one prefers this alternate definition of the ISI distribution, as in Gerstner and Kistler (2002), then one has

$$\hat{f}(\tau, t) = \int_{-\infty}^{\infty} h(t_s + \tau, t) \mathcal{W}(\tau, t_s, t - \tau) P^\dagger(t_s, t - \tau) dt_s, \quad (2.28)$$

implying that $\hat{f}(\tau, t) = f(\tau, t - \tau)$, and equation 2.27 becomes

$$\rho(\tau, t) = \frac{\hat{f}(\tau, t)}{\mathcal{F}(\tau, t - \tau)}. \quad (2.29)$$

2.2 Correlations. In this section, an expression for the joint serial ISI distribution, $f(\tau_{i+1}, \tau_i, t)$, will be derived for the proposed Markov process and shown to exhibit ISI correlations.

Recall the definition of the absence of correlations between two random variables: τ_i and τ_{i+1} are uncorrelated (independent) if and only if

$$f(\tau_{i+1}, \tau_i) = f(\tau_{i+1})f(\tau_i), \quad (2.30)$$

where $f(\tau_{i+1}, \tau_i)$ is the joint probability distribution of two back-to-back ISIs in the homogeneous case.

For the inhomogeneous case, a separation of this joint distribution $f(\tau_{i+1}, \tau_i, t)$ by Bayes' theorem,

$$f(\tau_{i+1}, \tau_i, t) = f(\tau_{i+1}, t | \tau_i) f(\tau_i, t - \tau_i), \quad (2.31)$$

reveals a subtlety: The time argument of $f(\tau_i, t)$, the marginal distribution of τ_i , must be retarded by τ_i . This is due to the fact that for τ_i to precede τ_{i+1} at t , it must occur at $t - \tau_i$. Given that $f(\tau, t)$ is known, it is left to determine an expression for $f(\tau_{i+1}, t | \tau_i)$. This can be achieved using equation 2.21 by replacing $P^*(t_s, t)$ with the conditional distribution of states just prior to spiking given a spike at $t - \tau_i$, which is denoted by $P^*(t_s, t | \tau_i)$.

The distribution $P^*(t_s, t | \tau_i)$, the conditional distribution of states just prior to spiking, given a spike at $t - \tau_i$, takes the form

$$P^*(t_s, t | \tau_i) = k_2 h(t_s, t) P(t_s, t | \text{spike at } t - \tau_i), \quad (2.32)$$

where k_2 is a normalization factor, and an expression for $P(t_s, t | \text{spike at } t - \tau_i)$ was given in equation 2.23. By inspection of equation 2.22, it can be seen that $k_2^{-1} = \rho(\tau_i, t)$. This results in

$$P^*(t_s, t | \tau_i) = \frac{h(t_s, t)\mathcal{W}(\tau_i, t_s - \tau_i, t - \tau_i)P^\dagger(t_s - \tau_i, t - \tau_i)}{f(\tau_i, t - \tau_i)}, \quad (2.33)$$

where the denominator, $\rho(\tau_i, t)\mathcal{F}(\tau_i, t - \tau_i)$, was replaced by $f(\tau_i, t - \tau_i)$ using equation 2.27.

Plugging this expression for $P^*(t_s, t | \tau_i)$ into equation 2.21 yields

$$\begin{aligned} f(\tau_{i+1}, \tau_i, t) &= \\ f(\tau_{i+1}, t | \tau_i)f(\tau_i, t - \tau_i) &= \int_{-\infty}^{\infty} h(\psi(t_s) + \tau_{i+1}, t + \tau_{i+1})\mathcal{W}(\tau_{i+1}, \psi(t_s), t) \\ &\times h(t_s, t)\mathcal{W}(\tau_i, t_s - \tau_i, t - \tau_i)P^\dagger(t_s - \tau_i, t - \tau_i)dt_s, \end{aligned} \quad (2.34)$$

an inhomogeneous expression for the joint ISI distribution of two successive ISIs.

It is instructive to verify that for the case of a renewal process, equation 2.34 predicts no correlations. For a renewal process, $\psi(t_s) = 0$ and $P^\dagger(t_s, t) = \delta(t_s)$, such that equation 2.34 becomes

$$f(\tau_{i+1}, \tau_i, t) = h(\tau_{i+1}, t + \tau_{i+1})\mathcal{W}(\tau_{i+1}, 0, t) \cdot h(\tau_i, t)\mathcal{W}(\tau_i, 0, t - \tau_i). \quad (2.35)$$

In addition, the ISI distribution given by equation 2.20 reduces to

$$f(\tau, t) = h(\tau, t + \tau)\mathcal{W}(\tau, 0, t). \quad (2.36)$$

Thus, it can be seen by inspection that equation 2.35 is of the form

$$f(\tau_{i+1}, \tau_i, t) = f(\tau_{i+1}, t)f(\tau_i, t - \tau_i), \quad (2.37)$$

implying as expected that successive ISIs are uncorrelated for a renewal process.

3 Connection to a Detailed Neuron Model

In this section we show that the full five-dimensional master equation for the canonical conductance-based integrate-and-fire neuron model driven by Poisson spike trains, augmented by mechanisms for SFA and a relative refractory period, can be reduced to a two-dimensional generalization of the 1DM model by an adiabatic elimination of fast variables.

3.1 Neuron Model, Adaptation, Input. Following Rudolph and Destexhe (2003a, 2005), Richardson (2004), Richardson and Gerstner (2005), we consider the equations for the membrane potential, $v(t)$, and excitatory and inhibitory synaptic conductances, $g_e(t)$ and $g_i(t)$, of the conductance-based integrate-and-fire neuron driven by Poisson spike trains:

$$c_m \frac{dv(t)}{dt} = g_l(E_l - v(t)) + g_e(t)(E_e - v(t)) + g_i(t)(E_i - v(t)) \quad (3.1)$$

$$\frac{dg_e(t)}{dt} = -\frac{1}{\tau_e} g_e(t) + q_e S_e(t) \quad (3.2)$$

$$\frac{dg_i(t)}{dt} = -\frac{1}{\tau_i} g_i(t) + q_i S_i(t), \quad (3.3)$$

where c_m represents the membrane capacitance, g_l the leak conductance, E_x the various reversal potentials, q_x the quantal conductance increases, and τ_x the synaptic time constants. The exact parameters used are given in appendix A. The excitatory and inhibitory input spike trains, $S_x(t)$ with $x \in \{e, i\}$, respectively, are given by

$$S_x(t) = \sum_k \delta(t - s_{x,k}), \quad (3.4)$$

where $s_{x,k}$ are the spike times of a realization of an inhomogeneous Poisson process (Papoulis & Pillai, 1991). Thus, $S_x(t)$ satisfies the constraints

$$\langle S_x(t) \rangle = v_x(t) \quad (3.5)$$

$$\langle S_x(t) S_x(t') \rangle = v_x(t) v_x(t') + v_x(t') \delta(t - t'). \quad (3.6)$$

Here $v_x(t)$ represents the time-varying rate of the inhomogeneous Poisson process, and $\langle \cdot \rangle$ represents the expectation value over the ensemble of realizations. In what follows, all Poisson processes are assumed inhomogeneous unless otherwise stated.

To put the neuron in a state of high conductance, it is bombarded by $N_e = 1000$ and $N_i = 250$ excitatory and inhibitory Poisson processes, all with rate functions $\lambda_e(t)$ and $\lambda_i(t)$, respectively, so that

$$v_x(t) = N_x \lambda_x(t). \quad (3.7)$$

A simple thresholding mechanism approximates the action potential dynamics of real neurons: If $v(t)$ exceeds the threshold, v_{th} , $v(t)$ is reset to v_{reset} . Analogous to the input spike train, we can thus define the output

spike train,

$$\mathcal{A}(t) = \sum_k \delta(t - s_k), \quad (3.8)$$

where s_k are the times of membrane potential threshold crossings enumerated by k .

SFA and a relative refractory period can both be modeled with the addition of a current to equation 3.1 of the form proposed in Dayan and Abbott (2001),

$$g_y(t)(E_y - v(t)), \quad (3.9)$$

where E_y is a reversal potential. The conductance $g_y(t)$ is governed by

$$\frac{dg_y(t)}{dt} = -\frac{1}{\tau_y}g_y(t) + q_y\mathcal{A}(t), \quad (3.10)$$

where τ_y and q_y are the time constant and quantal conductance increase of the mechanism. We label SFA and the relative refractory mechanism by the subscripts $y = s$ and $y = r$, respectively. Defining

$$\beta_v(v, g_e, g_i, g_s, g_r) := g_l(E_l - v) + \sum_{\mu=e,i,s,r} g_\mu(E_\mu - v) \quad (3.11)$$

and for $\mu = e, i, s, r$,

$$\beta_\mu(g_\mu) := -\frac{1}{\tau_\mu}g_\mu, \quad (3.12)$$

the five-dimensional system of coupled differential equations describing the conductance-based spike-frequency adapting relative refractory integrate-and-fire neuron driven by Poisson spike trains is:

$$c_m \frac{dv(t)}{dt} = \beta_v(v(t), \dots, g_r(t)) - (V_{\text{th}} - V_{\text{reset}})\mathcal{A}(t) \quad (3.13)$$

$$\frac{dg_x(t)}{dt} = \beta_x(g_x(t), t) + q_x\mathcal{S}_x(t) \quad (3.14)$$

$$\frac{dg_y(t)}{dt} = \beta_y(g_y(t), t) + q_y\mathcal{A}(t), \quad (3.15)$$

where $x \in \{e, i\}$ and $y \in \{s, r\}$. We refer to equations 3.13 to 3.15 as the full five-dimensional (5DF) model throughout the text (see the model overview in Table 1). The parameters used are given in Table 3.

3.2 Ensemble Behavior. It is natural to look for an ensemble description of equations 3.13 to 3.15, given that the input is described in terms of an ensemble.

Equations 3.13 to 3.15 are a set of concurrent first-order differential equations, that is, the right-hand sides at time t are functions of the instantaneous values of the state variables, $(v(t), g_e(t), g_i(t), g_s(t), g_r(t))$, implying no delays or memory effects are to be modeled. The system is therefore a Markov process, and given an initial distribution $P(v, g_e, g_i, g_s, g_r, t_0)$ for some t_0 , the evolution of $P(v, g_e, g_i, g_s, g_r, t)$ can be described by a suitable master equation (Risken, 1996). For the system in question here, the master equation takes the form

$$\begin{aligned} \frac{\partial}{\partial t} P(v, g_e, g_i, g_s, g_r, t) = & -\text{div} J(v, g_e, g_i, g_s, g_r, t) \\ & + \delta(v - v_{\text{reset}}) J_v(v_{\text{th}}, g_e, g_i, g_s - q_s, g_r - q_r, t), \end{aligned} \quad (3.16)$$

where the probability current density, J , is a vector with components

$$J_v(v, g_e, g_i, g_s, g_r, t) = \beta_v(v, g_e, g_i, g_s, g_r, t) P(v, g_e, g_i, g_s, g_r, t) \quad (3.17)$$

$$J_\mu := \beta_\mu(g_\mu, t) P(v, g_e, g_i, g_s, g_r, t) \quad (3.18)$$

with $\mu \in \{s, r\}$. (For J_e and J_i , see appendix B.) The δ term in equation 3.16 implements the reinsertion of probability flux that crosses the threshold. Furthermore, we define $P(v, g_e, g_i, g_s, g_r, t) = 0$ if one or more of the conductances g_e, \dots, g_r is negative.

There exists a wealth of literature treating master equations of conductance and current-based integrate-and-fire neuron models in the absence of adaptation and relative refractory mechanisms (Knight, 1972; Gerstner, 1995; Brunel, 2000; Omurtag et al., 2000; Nykamp & Tranchina, 2000; Knight, Omurtag, & Sirovich, 2000; Gerstner, 2000; Fourcaud & Brunel, 2002; Rudolph & Destexhe, 2003a; Richardson, 2004; Richardson & Gerstner, 2005). The usual approach is to make the so-called diffusion approximation yielding generally a Fokker-Planck equation for the membrane potential, and perhaps one or two other dimensions treating synaptic conductances.

We present here a novel approach applicable for neurons in the high-conductance state whereby the variables v, g_e, g_i are eliminated by a technique known as an adiabatic elimination of fast variables (Haken, 1983; Gardiner, 1984), and the system is reduced to a master equation for the two-dimensional marginal probability distribution, $P(g_s, g_r, t)$, of the slow variables, g_s and g_r . As we will see, the membrane potential, v , and the synaptic conductances, g_e and g_i , are thus encapsulated in the hazard function, $h_g(g_s, g_r, t)$. We treat here the static input case, λ_e, λ_i . The case for dynamic external input $\lambda_e(t), \lambda_i(t)$ is treated in section 4.

We follow here the intuitive treatment of adiabatic elimination given in Haken (1983). We begin by integrating $P(v, \dots, g_r)$ over the fast variables v, g_e, g_i , yielding the marginal distribution for the slow variables g_s, g_r ,

$$P(g_s, g_r, t) = \int_0^\infty \int_0^\infty \int_{-\infty}^{v_{\text{th}}} P(v, g_e, g_i, g_s, g_r, t) dv dg_e dg_i. \quad (3.19)$$

Integrating equation 3.16 over v, g_e, g_i yields

$$\begin{aligned} \frac{\partial}{\partial t} P(g_s, g_r, t) &= - \sum_{\mu=s,r} \frac{\partial}{\partial g_\mu} (\beta_\mu(g_\mu) P(g_s, g_r, t)) \\ &\quad - \int_0^\infty \int_0^\infty \beta_v(v_{\text{th}}, g_e, g_i, g_s, g_r) P(v_{\text{th}}, g_e, g_i, g_s, g_r, t) dg_e dg_i \\ &\quad + \int_0^\infty \int_0^\infty \beta_v(v_{\text{th}}, g_e, g_i, g_s - q_s, g_r - q_r) \\ &\quad \times P(v_{\text{th}}, g_e, g_i, g_s - q_s, g_r - q_r, t) dg_e dg_i. \end{aligned} \quad (3.20)$$

For details of the calculation, see appendix B. Now we separate the marginal distribution for the slow variables from the full distribution by Bayes' theorem, resulting in

$$P(v, g_e, g_i, g_s, g_r, t) = P(v, g_e, g_i, t | g_s, g_r, t) P(g_s, g_r, t), \quad (3.21)$$

and make the adiabatic approximation as in Haken (1983) that

$$P(v, g_e, g_i, t | g_s, g_r, t) \approx P^{(g_s, g_r)}(v, g_e, g_i, t), \quad (3.22)$$

where $P^{(g_s, g_r)}(v, g_e, g_i, t)$ is the solution to the three-dimensional master equation for the canonical conductance-based integrate-and-fire neuron with a constant bias current, $I(g_s, g_r) = g_s(E_s - v) + g_r(E_r - v)$, with neither SFA nor the relative refractory mechanism. This implies we assume that v, g_e, g_i are immediately at equilibrium given the slow variables, or in other words, the system responds adiabatically to the dynamics of the slow variables g_s, g_r . The adiabatic assumption ensures the two-dimensional process $(g_s(t), g_r(t))$ is a Markov process.

Now defining the hazard function,

$$h_g(g_s, g_r, t) := \int_0^\infty \int_0^\infty \beta_v(v_{\text{th}}, g_e, g_i, g_s, g_r) P^{(g_s, g_r)}(v_{\text{th}}, g_e, g_i, t) dg_e dg_i, \quad (3.23)$$

the master equation, 3.20, becomes

$$\begin{aligned} \frac{\partial}{\partial t} P(g_s, g_r, t) = & - \sum_{\mu=s,r} \frac{\partial}{\partial g_\mu} (\beta_\mu(g_\mu) P(g_s, g_r, t)) \\ & - h_g(g_s, g_r, t) P(g_s, g_r, t) \\ & + h_g(g_s - q_s, g_r - q_r, t) P(g_s - q_s, g_r - q_r, t). \end{aligned} \quad (3.24)$$

We refer to the model defined by equation 3.24 as the 2D Markov (2DM) model throughout the text (see the model overview in Table 1). Since no analytical solution is yet known for $P^{(g_s, g_r)}(v_{th}, g_e, g_i, t)$ in equation 3.23, $h_g(g_s, g_r)$ was extracted from Monte Carlo simulations of equations 3.13 to 3.15, as will be discussed in section 4.1. Then given a solution to the master equation, $P(g_s, g_r, t)$, the firing rate of the ensemble, denoted by $\alpha(t)$, is determined by the expectation value of the hazard function $h_g(g_s, g_r, t)$ over $P(g_s, g_r, t)$:

$$\alpha(t) = \int_0^\infty \int_0^\infty h_g(g_s, g_r, t) P(g_s, g_r, t) dg_s dg_r. \quad (3.25)$$

For the adiabatic approximation, the assumption that g_s is slow compared to v, g_e, g_i is easily justified as the timescale of g_s is on the order of 100 ms, while the timescale of v is on the order of 2 ms in the high-conductance state. The timescale of the mean and standard deviation of g_e and g_i are on the order of $\tau_e = 1.5$ ms and $\tau_i = 10$ ms, respectively, while the fluctuations of g_e and g_i are the source of stochasticity of the system and are on a still shorter timescale.

The timescale of g_r is significantly faster than g_s , though its treatment as a slow variable is also justifiable, but in a somewhat indirect manner. As has been argued in Fourcaud and Brunel (2002) and Renart et al. (2004), for neurons with synaptic time constants comparable to or larger than the effective membrane time constant and driven by sufficient input noise, as is the case here, the firing rate follows the input current almost instantaneously. It is this property that allows the dynamic firing rate to be treated as a function of the time-dependent means and variances of the synaptic conductances in La Camera et al. (2004), a method we follow in section 4. This suggests that such modulations do not push the system far from equilibrium and that the system returns to equilibrium on a timescale faster than that of the synaptic means (τ_e, τ_i). Since over the domain of the g_r trajectory for which the integrals on the right-hand side of equation 3.20 are nonzero, g_r has a timescale comparable to the mean of the synapses, the argument applies equally to g_r . However, since g_r is spike triggered, we leave g_r in the master equation, while the synaptic variables, g_e and g_i , determine $h_g(g_s, g_r, t)$ and can be treated outside the master equation formalism.

Methods to undertake a rigorous analysis of the error in the adiabatic approximation are beyond the scope of this letter. What follows are a variety of numerical comparisons to demonstrate the accuracy and domain of applicability of the proposed approximation.

4 Methods

In this section we provide methods for determining appropriate homogeneous and inhomogeneous hazard functions for the 1DM, 2DM, and renewal models. Since no analytical expression for equation 3.23, or the renewal hazard function of the 5DF model is yet known, we approach the problem by fitting the homogeneous hazard functions determined by 5DF Monte Carlo simulations in the static case. The inhomogeneous functions are then constructed from the homogeneous ones by discretizing time and taking one homogeneous hazard function for the duration of a single time bin.

4.1 Determining the Static Hazard Function for Markov Models.

Given a finite subset of the possible realizations of the Poisson input spike trains, the 5DF model equations, 3.13 to 3.15, can be integrated for each input realization. Any statistical quantity of interest can then be approximated by averaging or histogramming over this finite set of trajectories. This approach is known as the Monte Carlo method. By increasing the number of trials in this finite set of realizations, the statistical quantities determined by the Monte Carlo method converge to the true quantities. Therefore, Monte Carlo simulations are used for determining the unknown hazard functions as well as later benchmarking the reduced master equations.

By Monte Carlo simulations of the 5DF model under static stimulation, the quantities $P^*(g_s + g_r)$, $P(g_s + g_r)$, and $\alpha(t)$ can be obtained. Then analogous to equation 2.16, we can determine $h_g(g_s, g_r)$ by

$$h_g(g_s, g_r) = h_g(g_s + g_r) = \frac{\alpha P^*(g_s + g_r)}{P(g_s + g_r)}, \quad (4.1)$$

where we treat the sum of the conductances, $g_s + g_r$, rather than each independently because we have chosen their reversal potentials to be equal (see appendix A). It was found that $h_g(g_s, g_r)$ can be fit well by a function of the form

$$h_g(g_s, g_r) = a \exp(-b \cdot (g_s + g_r)), \quad (4.2)$$

where a and b are fit parameters. Some typical fits for various excitatory Poisson input rates are shown in Figure 1. For the 1DM model, the same fit parameters were used, but with $g_r = 0$. Transforming to (t_s, t_r) by the

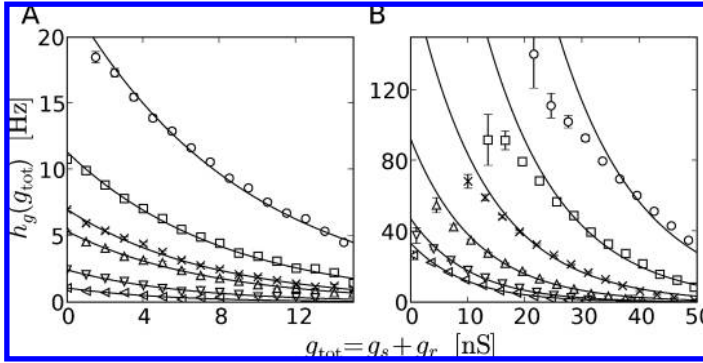


Figure 1: $h_g(g_s, g_r) = h_g(g_s + g_r)$ as a function of $g_{\text{tot}} = g_s + g_r$, as determined from 5DF Monte Carlo (data points, 1000 trials per λ_e , 10 s per trial, $dt = 0.01$ ms) by equation 4.1, was found to be approximately exponential for a range of excitatory stimulation rates, λ_e , with the inhibitory stimulation rate fixed at $\lambda_i = 11.4$ Hz. For the definition of the 5DF model, see Table 1. The exponential fits (lines) are good for low rates ($\triangleleft: \lambda_e = 5.26$ Hz, $\nabla: \lambda_e = 5.56$ Hz, $\triangle: \lambda_e = 5.88$ Hz, $\times: \lambda_e = 6.01$ Hz, $\square: \lambda_e = 6.25$ Hz, $\circ: \lambda_e = 6.67$ Hz) in A, but poorer for g_s near zero for high rates ($\triangleleft: \lambda_e = 6.90$ Hz, $\nabla: \lambda_e = 7.14$ Hz, $\triangle: \lambda_e = 7.69$ Hz, $\times: \lambda_e = 8.33$ Hz, $\square: \lambda_e = 9.09$ Hz, $\circ: \lambda_e = 10.0$ Hz) in B.

inverse of equation 2.5, we have

$$h(t_s, t_r) = a \exp \left(-b \cdot \left(q_s \exp \left(\frac{-t_s}{\tau_s} \right) + q_r \exp \left(\frac{-t_r}{\tau_r} \right) \right) \right). \quad (4.3)$$

4.2 Constructing Inhomogeneous Hazard Functions. Now given the hazard functions determined under static input statistics, the inhomogeneous hazard function given time-varying Poisson input rates $\lambda_e(t)$, $\lambda_i(t)$ can be constructed by accounting for synaptic filtering.

The homogeneous hazard functions given static stimulation rates λ_e , λ_i determined by the recipes in section 4.1 are the hazard functions given synaptic conductance distributions parameterized by $\langle g_{e,i} \rangle$, neglecting higher-order moments. It can be shown that

$$\frac{d}{dt} \langle g_x(t) \rangle = -\frac{1}{\tau_x} (\langle g_x(t) \rangle - q_x \tau_x N_x \lambda_x(t)), \quad (4.4)$$

with $x \in \{e, i\}$, a low-pass filter equation of the quantity $q_x \tau_x N_x \lambda_x(t)$ with a cutoff frequency of $2\pi/\tau_x$ (Gardiner, 1985; La Camera et al., 2004).

As argued in Fourcaud and Brunel (2002) and Renart et al. (2004), the firing rate of neurons with nonzero synaptic time constants driven by

sufficient noise follows their input currents instantaneously. Then the hazard function $h_g(g_s, g_r, t)$ here is also determined instantaneously by the mean synaptic conductances. Therefore, inhomogeneous parameters $a(t)$ and $b(t)$ in equation 4.3 can be determined by interpolating the parameters determined from static $\langle g_e \rangle$ and $\langle g_i \rangle$ with the instantaneous dynamic $\langle g_e(t) \rangle$ and $\langle g_i(t) \rangle$ determined by integrating equation 4.4 for some given arbitrary time-varying input spike trains parameterized by $\lambda_e(t)$, $\lambda_i(t)$. Thus, we have the hazard function

$$h_g(g_s, g_r, t) = a(t) \exp(-b(t) \cdot (g_s + g_r)). \quad (4.5)$$

A similar approach was taken in La Camera et al. (2004), except that we do not correctly account for the dynamics of the standard deviation of the synaptic conductance by the fitting approach used here. This could be remedied given an analytically solvable neuron model as was used in La Camera et al.

In this study, we investigate only time-varying excitation. Treating inhibition in addition would require additional fits and two-dimensional interpolation of the resulting parameters but would yield no new results for this study.

4.3 Comparing to Renewal Theory Models. In inhomogeneous renewal theory, only the time since the last spike (age) enters into the hazard function (Gerstner & Kistler, 2002). While such theories cannot account for ISI correlations due to SFA, they can account for much of the gradual increase in excitability that follows a spike due to SFA by an appropriately chosen hazard function. Perhaps surprisingly, such models are sufficient to exhibit “adapting” transients to step stimuli. Like the 2DM model, we seek to calibrate such renewal models to the 5DF system and assess their suitability for modeling the ensemble firing rate under dynamic stimuli. Sufficient for such a comparison is a recipe for specifying the hazard function as a function of the static stimulus. The dynamic case can then be constructed by using the effective synaptic filtered stimulus to determine the inhomogeneous hazard function at each instant in time, as for the Markov models in the previous section.

For the static case, one can determine the hazard function as a function of the stimulus by interpolating the ISI distribution due to 5DF Monte Carlo and applying the standard renewal theory result that

$$\rho(\tau) = \frac{f(\tau)}{\mathcal{F}(\tau)}, \quad (4.6)$$

where the renewal theory survival function is given by

$$\mathcal{F}(\tau) = \int_{s=\tau}^{\infty} f(s)ds. \quad (4.7)$$

The renewal model will thus reproduce the ISI distribution of 5DF Monte Carlo under static stimulation. This process is numerically unstable for large τ , and for the dynamic case too costly. Another approach is to determine the renewal hazard function by equation 2.26, with one caveat: since the resulting renewal hazard function must be uniquely determined by the stimulus, $P(t_s, t_r, t)$ in equation 2.26 must be replaced by $P_{\infty}(t_s, t_r, t)$, the instantaneous equilibrium distribution, or asymptotic state distribution for large time resulting from a $h(t_s, t_r, t)$ fixed at the instantaneous value at time t . The renewal hazard function determined by this recipe, combined with the renewal master equation C.7, defines what we subsequently refer to as the effective renewal (ER) model (see the model overview in Table 1). Typical hazard functions are shown in Figure 2. Indeed, the renewal hazard functions determined by equation 2.26 are consistent with those of 5DF Monte Carlo determined by equation 4.6.

Simulation of the ER model implies that the master equation for $P(t_s, t_r, t)$ must be allowed to converge to $P_{\infty}(t_s, t_r, t)$ for each time step where the stimulation changes. This is costly and makes the ER models much less efficient to simulate than the 1DM and 2DM models, but allows a direct comparison of renewal models with the 1DM and 2DM models and 5DF Monte Carlo. When the renewal hazard function is known a priori, as would be the case for a gamma renewal process, or when the hazard functions can be fit by simple functions, the renewal theory ensemble equations given in appendix C are comparatively more efficient to simulate than the 1DM and 2DM models.

5 Numerics

In this section we describe the numerical techniques applied to solve the 1DM and 2DM master equations, generate realizations of the 1DM and 2DM processes, and solve the 5DF neuron model equations.

5.1 Numerical Solution of Master Equations. We solved the 1DM and 2DM master equations numerically by discretizing $P(t_s, t)$ and $P(t_s, t_r, t)$, respectively, applying the exponential Euler method for the death term, and reinserting the lost probability by walking the negative time domain and fetching the probability sources of each bin determined by equation 2.8. We present the one-dimensional case here, which can be generalized to two dimensions.

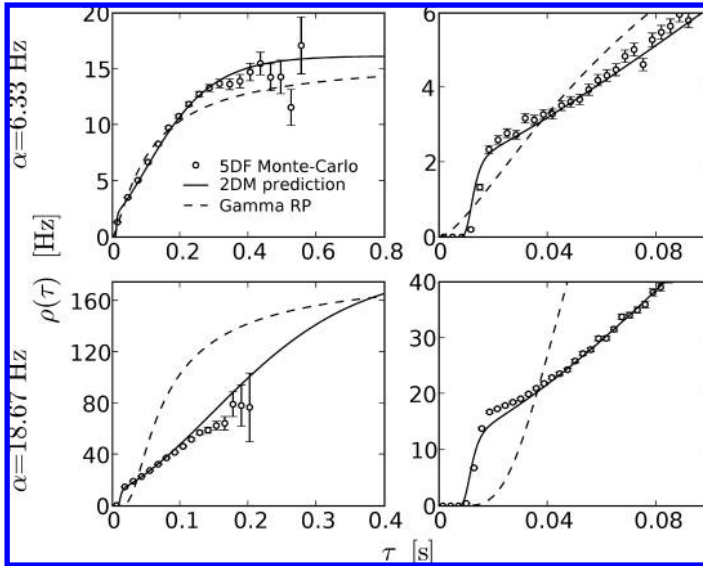


Figure 2: The renewal hazard function, $\rho(\tau)$, for synaptic input rates ($\lambda_e = 6.5$ Hz, $\lambda_i = 11.4$ Hz) and ($\lambda_e = 8.3$ Hz, $\lambda_i = 11.4$ Hz) resulting in an ensemble firing rate of $\alpha = 6.33$ Hz (top row), and $\alpha = 18.67$ Hz (bottom row), respectively. The renewal hazard function for 5DF Monte Carlo (circles) was computed by equation 4.6 with a spike train of 10^4 s. The renewal hazard function due to the 2DM model (solid line) was determined by equation 2.26. The renewal hazard function for a gamma renewal process (dashed line) equal to the 2DM renewal hazard function at large τ and with the same average firing rate was computed as discussed in section C.2. The small τ region is shown blown up in the right column. For the definition of the 2DM and 5DF models, see Table 1.

We discretize $P(t_s, t)$ on equally spaced grids t_s^i and t^j with grid spacings $\Delta t_s := t_s^{i+1} - t_s^i$ and $\Delta t := t^{j+1} - t^j$, respectively, with $\Delta t_s = \Delta t$, such that $P(t_s, t) \rightarrow P^{i,j}$. The discretized form of the master equation 2.9 then takes the form

$$P^{i+1,j+1} = P^{i,j} \exp(-\Delta t \cdot h(t_s^i, t^j)) + P_r^{i,j}, \quad (5.1)$$

where the first term is the exponential Euler computation of loss of probability due to the death term. On the left-hand side, the first superscript of P , $i + 1$, leads i by one to implement the constant drift of t_s , $dt_s/dt = 1$. The

Table 1: Overview of the Models and Quick Reference for the Equations and Sections for the Models.

Model	Description	Keywords	Defined in (section)	Equations	Calibration to 5DF Recipe in (section)	Numerics in (section)
1DM	One-dimensional Markov process	Beyond renewal theory, spike-frequency adaptation, master equation, ensemble	2	2.4, 2.9	4.1, 4.2	5.1 (master equation), 5.3 (realizations)
5DF	Conductance-based spike-frequency adapting relative refractory integrate-and-fire neuron driven by Poisson spike trains	Full five-dimensional system, Monte Carlo, reference, benchmark	3.1, A	3.13–3.15	NA	5.2
2DM	Two-dimensional Markov process	Adiabatic elimination (of 5DF), spike-frequency adaptation, relative refractory period, master equation, ensemble	3.2	3.24	4.1, 4.2	5.1 (master equation), 5.3 (realizations)
ER	Effective renewal theory model	Inhomogeneous, master equation	C	C.7	4.3, 4.2	C.1 (master equation), C.2 (realizations)

reinserted probability, $P_r^{i,j}$, is computed for $t_s^i + \Delta t_s < 0$ by

$$\begin{aligned}
 P_r^{i,j} := & \sum_{m=i_{\text{rif}}(t_s^i)}^{i_{\text{rif}}(t_s^{i+1})-1} P_d^{m,j} \\
 & + \frac{\psi^{-1}(t_s^{i+1}) - i_{\text{rif}}(t_s^{i+1})}{\Delta t_s} P_d^{i+1,j} \\
 & - \frac{\psi^{-1}(t_s^i) - i_{\text{rif}}(t_s^i)}{\Delta t_s} P_d^{i,j},
 \end{aligned} \tag{5.2}$$

where $P_d^{i,j}$ is the loss of probability computed by

$$P_d^{i,j} := \Delta t \cdot P^{i,j} \cdot h(t_s^i, t^j), \tag{5.3}$$

and i_{rif} refers to the “reinserted-from” index, which satisfies

$$t_s^{i_{\text{rif}}(t_s^i)} \leq \psi^{-1}(t_s^i) < t_s^{i_{\text{rif}}(t_s^i)} + \Delta t_s. \tag{5.4}$$

The first term in equation 5.2 is just a sum of all $P_d^{i,j}$ except the fractional last bin, which sends probability to the interval $t \in [t_s^i, t_s^i + \Delta t_s)$. The second two terms subtract the fractional first and add the fractional last bins of $P_d^{i,j}$, which are reinserted to the interval, and thus implement a sort of anti-aliasing of the reinsertion mapping.

5.2 Neuron Simulations. Monte Carlo simulations of the full-system (5DF Monte Carlo) were performed by solving equations 3.13 to 3.15 using the NEST simulation environment (Diesmann & Gewaltig, 2002) with a time step of 0.01 ms.

5.3 Generating Realizations of the Proposed Markov Processes. Generating realizations of the proposed 1DM or 2DM processes is straightforward: The thinning method for a general hazard function described in Devroye (1986) can be applied. The quantity $h_{\text{max}} = \max_{t_s,t}(h(t_s, t))$ for the 1DM case or $h_{\text{max}} = \max_{t_s,t_r,t}(h(t_s, t_r, t))$ for the 2DM case must be known. The variables t and t_s (1DM), or t, t_s , and t_r (2DM) are required and can have initial values of zero. Sequential intervals are generated using a homogeneous Poisson process with hazard rate $\rho = h_{\text{max}}$. Given one such interval, Δt_i , it is added to t and t_s (1DM), or t, t_s , and t_r (2DM). Next, a spike is generated at time t with probability $h(t_s, t)/h_{\text{max}}$ (1DM) or $h(t_s, t_r, t)/h_{\text{max}}$ (2DM), and if a spike is generated, $t_s \mapsto \psi_s(t_s)$, and $t_r \mapsto \psi_r(t_r)$, where ψ_s and ψ_r refer to the reinsertion mappings as in equation 2.7 with the respective parameters for the two mechanisms.

6 Results

In this section we compare ISI distributions, static ISI correlations, and firing rate dynamics of the 1DM, 2DM, and ER models to 5DF Monte Carlo.

6.1 Interspike Interval Distributions. The predictions due to the ER and 2DM model are in excellent agreement with the static ISI distribution of 5DF Monte Carlo. The prediction due to the 1DM model neglects refractory effects and is therefore poor for low ISIs, as can be seen in Figure 3.

6.2 Interspike Interval Correlations. In this section we investigate correlations between subsequent ISIs, a feature of the proposed 1DM and 2DM models that is absent by definition in renewal theory models of spike statistics.

The correlation coefficient, r , for a finite number of observations is defined by

$$r^2 = \frac{(\sum(x_i - \bar{x})(y_i - \bar{y}))^2}{\sum(x_i - \bar{x})^2 \sum(y_i - \bar{y})^2}, \quad (6.1)$$

and is the standard measure by which to quantify correlations between two random variables x , y , where x_i , y_i denote the individual observations and \bar{x} , \bar{y} denote the means.

The correlation coefficients of subsequent ISIs under static stimulation were calculated for 100 runs of 100 s, and the mean and deviation in the mean are given in Table 2. Indeed, the renewal process shows no ISI correlations. For low and high firing rates, the difference between the correlation coefficients for 5DF Monte Carlo and realizations of the 2DM model is consistent with zero. Both exhibit negative ISI correlations, implying short ISIs are generally followed by long ISIs and vice versa, as has been observed in previous experimental and theoretical studies (Longtin & Racicot, 1997; Chacron, Longtin, & Maler, 2000; Chacron et al., 2005; Nawrot et al., 2007).

The conditional ISI distribution, $f(\tau_{i+1}|\tau_i)$ can be computed for the 1DM and 2DM models by equation 2.34. Predictions due to the 2DM model are in agreement with 5DF Monte Carlo for low and high rates, and both long and short τ_i , as shown in Figure 3. Applying equation 2.34, we can compute the quantity

$$\langle \tau_{i+1} | \tau_i \rangle_{\tau_{i+1}} = \int_0^\infty \tau_{i+1} f(\tau_{i+1} | \tau_i) d\tau_{i+1}. \quad (6.2)$$

As discussed in Whittaker and Robinson (1967), this is a linear function of τ_i for normal distributions, the slope of which is the correlation coefficient. As the ISI distributions here are not normal, there are deviations from linearity,

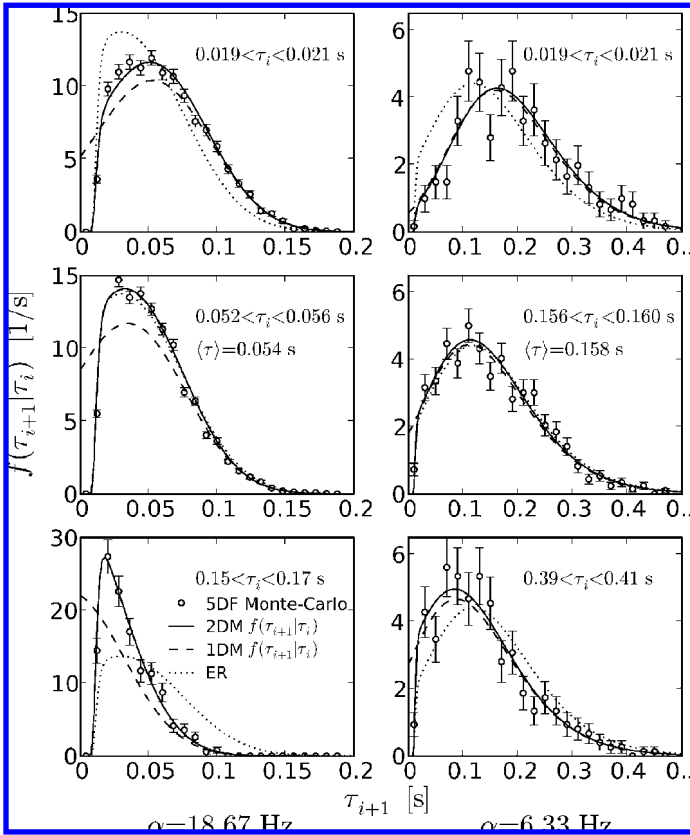


Figure 3: Comparison of the conditional ISI distributions due to 5DF Monte Carlo with predictions due to effective renewal theory (ER, dotted line), the 1DM model (dashed line, determined by equation 2.34), and the 2DM model (solid line, determined by the 2D generalization of equation 2.34). For the definition of the 1DM, 2DM, 5DF, and ER models, see Table 1. The left column shows three representative conditional ISI distributions for an ensemble firing rate of $\alpha = 18.67$ Hz ($\lambda_e = 8.3$ Hz, $\lambda_i = 11.4$ Hz), and the right column shows the same for $\alpha = 6.33$ Hz ($\lambda_e = 6.5$ Hz, $\lambda_i = 11.4$ Hz). The upper two plots show the conditional ISI distribution for τ_i much shorter than the mean. The middle two plots show the conditional ISI distribution for τ_i equal to the mean. The lower two plots show the conditional ISI distribution for τ_i much longer than the mean. The preceding ISI, τ_i , is given on each plot, and a small interval around τ_i is used to compute the distributions from 5DF Monte Carlo to yield sufficient statistics. The theoretical predictions of the conditional ISI distributions using the 2DM model are in good agreement with 5DF Monte Carlo for all situations considered. The ISI distribution due to 5DF Monte Carlo is consistent with the renewal ISI distribution only when the preceding ISI is equal to the mean ISI (middle row). Spike trains of duration 10^4 s were used. Error bars represent the relative error in the histogram bin counts, $1/\sqrt{\text{count}}$.

Table 2: Serial ISI Correlation Coefficients for Monte Carlo Simulations of the Full Five-Dimensional System (5DF), Realizations of the One- and Two-Dimensional Markov Models (1DM, 2DM), and Realizations of the Effective Renewal Theory Model (ER).

Model	Correlation coefficient
$\alpha = 6.33$ Hz	
5DF	-0.148 ± 0.004
2DM	-0.147 ± 0.003
1DM	-0.160 ± 0.003
ER	0.0042 ± 0.0043
$\alpha = 18.67$ Hz	
5DF	-0.235 ± 0.002
2DM	-0.236 ± 0.002
1DM	-0.283 ± 0.002
ER	0.001 ± 0.002

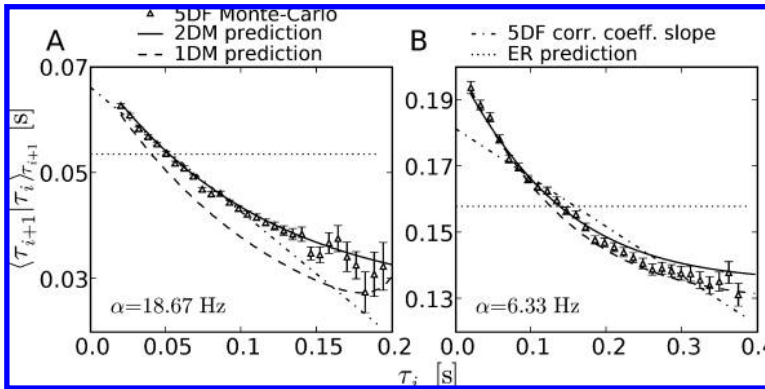


Figure 4: Mean of the conditional ISI distribution as a function of the preceding ISI, τ_i , for high-ensemble firing rates (A, ($\lambda_e = 8.3$ Hz, $\lambda_i = 11.4$ Hz), $\alpha = 18.67$ Hz) and low-ensemble firing rates (B, ($\lambda_e = 6.5$ Hz, $\lambda_i = 11.4$ Hz), $\alpha = 6.33$ Hz). The data points (triangles) shown are for 5DF Monte Carlo. Theoretical predictions due to the 1DM (dashed line), 2DM (solid line), and ER (dotted line) models are shown. For the definition of the 1DM, 2DM, 5DF, and ER models, see Table 1. A linear function with slope equal to the serial ISI correlation coefficient would be the functional form if the ISI distributions were normal. Thus, these linear functions are plotted for comparison.

as shown in Figure 4. Predictions due to equation 6.2 for the 2DM model are consistent with 5DF Monte Carlo for both low and high rates, as seen in Figure 4. Thus, the 2DM model is indistinguishable from the full system when considering static correlations.

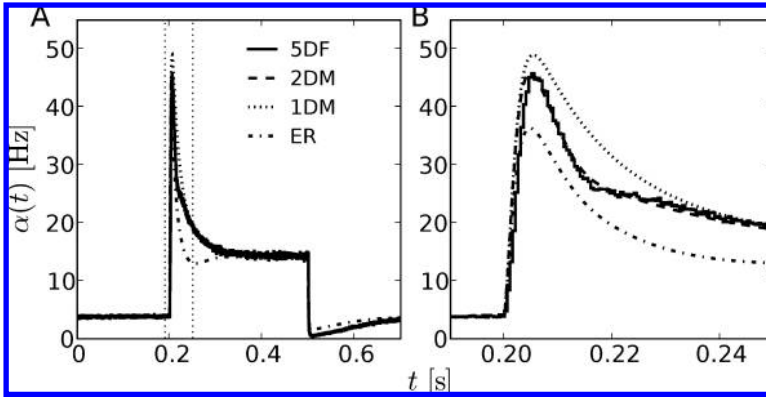


Figure 5: (A) The ensemble firing rate, $\alpha(t)$, in response to a moderate step stimulus, determined by 5DF Monte Carlo ($5 \cdot 10^5$ trials, solid line), and numerical solution of the 1DM (dotted line), 2DM (dashed line), and ER (dashed dotted line) master equations. For the definition of the 5DF, 1DM, 2DM, and ER models, see Table 1. (B) The region outlined by the dashed rectangle is enlarged, showing consistency between the two-dimensional Markov (2DM) model and the full system (5DF Monte Carlo) apart from a 0.5 ms lead of the 2DM solution. This discrepancy is likely due to the neglected membrane potential dynamics.

6.3 Firing Rate Dynamics. In this section, we compare the ensemble firing rates of the 1DM, 2DM, and ER models to 5DF Monte Carlo for small to large step stimuli, and for random fluctuating stimuli generated by an Ornstein-Uhlenbeck process.

We subject the neural ensemble to a dynamic stimulus by specifying a time-varying excitatory Poisson input rate, $\lambda_e(t)$. Given the time-dependent hazard function determined by the Poisson input rates as described in section 4.2, the ensemble firing rate, $\alpha(t)$, of the 1DM and 2DM models can be calculated by solving equations 2.9 and 3.24, respectively, for the time-dependent state distribution, and subsequently applying equation 2.17 or the 2D generalization of it. For the ER model, the hazard function was calculated by the methods discussed in section 4.3, and the ensemble firing rate was determined by solving equation C.7.

For weak step stimuli that do not bring the system too far from equilibrium, all models (ER, 1DM, 2DM) faithfully reproduce the step stimulus response of 5DF Monte Carlo (not shown). For moderate step stimuli, only the 2DM model faithfully reproduces the step stimulus response of 5DF Monte Carlo, shown in Figure 5. For large step stimuli, the 2DM model starts to deviate from 5DF Monte Carlo, as seen in Figure 6.

The effective renewal theory (ER) model does a reasonable job of predicting the ensemble firing rate of the system to low-amplitude step stimuli.

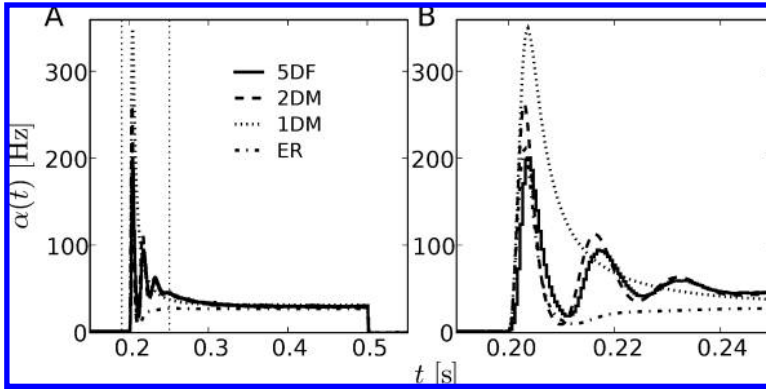


Figure 6: (A) The ensemble firing rate, $\alpha(t)$, in response to a large step stimulus, determined by 5DF Monte Carlo ($5 \cdot 10^5$ trials, solid line), and numerical solution of the 1DM (dotted line), 2DM (dashed line), and ER (dashed dotted line) master equations. For the definition of the 5DF, 1DM, 2DM, and ER models, see Table 1. (B) The region outlined by the dashed rectangle is enlarged, showing disagreement between the two-dimensional Markov (2DM) model and the full system (5DF Monte Carlo).

This is perhaps surprising, since we do not expect renewal models to faithfully reproduce the dynamical responses of spike-frequency adapting neurons, as renewal models do not account for the dependencies of the firing probability density (hazard function) on spikes prior to the most recent. However, this shows that if the ensemble is not pushed far from equilibrium, knowledge of just the last spike is sufficient to predict the firing rate.

We further compared 5DF Monte Carlo and predictions of the 2DM model for a stimulus, $v_e(t)$, generated by an Ornstein-Uhlenbeck (OU) process. Let $\zeta(t)$ be an OU process with mean of 10 Hz, standard deviation of 0.6 Hz, and time constant of 0.2 s. Then the excitatory synaptic inputs were supplied with $v_e(t) = N_e \zeta(t)$, with $N_e = 1000$ being the number of excitatory synaptic inputs.

The ensemble firing rates for the 2DM model, its adiabatic solution, and 5DF Monte Carlo are shown in Figure 7. The adiabatic solution of the 2DM model is defined as the system that at each instant in time has a distribution of states equal to the instantaneous equilibrium distribution, $P_\infty(t_s, t_r, t)$, the asymptotic state distribution for large time resulting from a $h(t_s, t_r, t)$ fixed at the instantaneous value at time t . The firing rate of the adiabatic 2DM model is then calculated by

$$\alpha(t) = \int_{-\infty}^{\infty} h(t_s, t_r, t) P_\infty(t_s, t_r, t) dt_s dt_r. \quad (6.3)$$

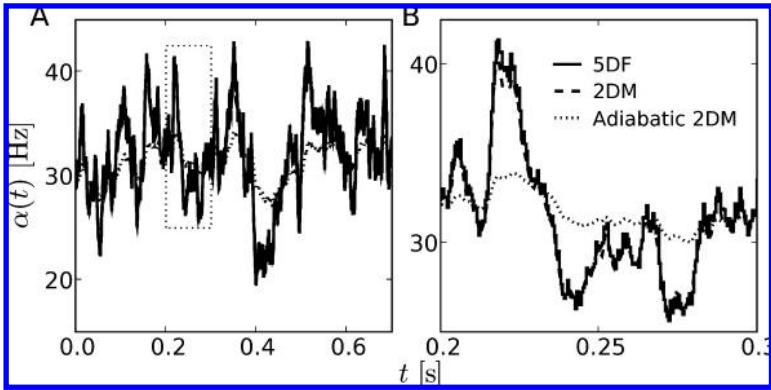


Figure 7: (A) The ensemble firing rate, $\alpha(t)$, in response to an Ornstein-Uhlenbeck process stimulus (as described in the text), determined by 5DF Monte Carlo (solid line), numerical solution of the 2DM master equation (dashed line), and the adiabatic solution (adiabatic 2DM, dotted line) computed by equation 6.3. For the definition of the 5DF, and 2DM models, see Table 1. (B) The region outlined by the dashed rectangle is enlarged, showing consistency between the two-dimensional Markov (2DM) model and the full system (5DF Monte Carlo).

By comparison of the ensemble firing rates of the 2DM model with its adiabatic solution in Figure 7, we can see that the system is being driven from equilibrium by the stimulus. Furthermore, the behavior of the 2DM model far from equilibrium captures the ensemble firing rate dynamics of 5DF Monte Carlo faithfully. This is a robust result under variation of neuron parameters and stimuli, so long as the ensemble is not pushed too far from equilibrium, as for the large step stimulus in Figure 6.

7 Beyond Mean-Adaptation Approximations

In this section we show that statistical moment theory approximations such as the mean-adaptation theories due to La Camera et al. (2004) can be derived from the 1DM master equation. The approach generalizes, and we derive the next order moment theory approximation, a mean+variance-adaptation theory and use it to clarify the domain of validity of mean-adaptation theories.

Recall the 1DM master equation for a spike-frequency adapting neuron,

$$\begin{aligned} \frac{\partial}{\partial t} P(g_s, t) &= \frac{\partial}{\partial g_s} \left[\frac{g_s}{\tau_s} P(g_s, t) \right] \\ &\quad + h_g(g_s - q_s, t) P(g_s - q_s, t) \\ &\quad - h_g(g_s, t) P(g_s, t), \end{aligned} \tag{7.1}$$

where $P(g_s, t)$ is the probability density of the adaptation state variable, g_s , and $P(g_s < 0, t) = 0$. The ensemble firing rate, $\alpha(t)$, is given by

$$\alpha(t) = \int_{-\infty}^{\infty} h_g(g_s, t)P(g_s, t)dg_s. \quad (7.2)$$

The mean adaptation variable is

$$\langle g_s(t) \rangle = \int_{-\infty}^{\infty} g_s P(g_s, t)dg_s. \quad (7.3)$$

Multiplying equation 7.1 by g_s and integrating over g_s yields the time evolution of the mean, $\langle g_s(t) \rangle$,

$$\frac{d\langle g_s(t) \rangle}{dt} = -\frac{1}{\tau_s} \langle g_s(t) \rangle + q_s \alpha(t). \quad (7.4)$$

By Taylor expanding $h_g(g_s)$ in equation 7.2 around $\langle g_s(t) \rangle$, and keeping up to linear terms, a mean-adaptation theory as in La Camera et al. (2004) results. Keeping up to quadratic terms, we have

$$\alpha(t) \approx \alpha(\langle g_s(t) \rangle, \langle \Delta g_s^2(t) \rangle) = h_g(\langle g_s(t) \rangle) - \frac{1}{2} h_g''(\langle g_s(t) \rangle) \cdot \langle \Delta g_s^2(t) \rangle, \quad (7.5)$$

where the $h_g'(\langle g_s(t) \rangle)$ term vanishes by a cancellation of means. A mean+variance-adaptation theory results, but we require the time evolution of the variance. Multiplying equation 7.1 by $(g_s - \langle g_s(t) \rangle)^2$ and integrating over g_s yields the time evolution of the variance, $\langle \Delta g_s^2(t) \rangle$,

$$\begin{aligned} \frac{d\langle \Delta g_s^2(t) \rangle}{dt} &= -\frac{2}{\tau_s} \langle \Delta g_s^2(t) \rangle + q_s^2 \alpha(t) \\ &\quad + 2q_s \int_0^{\infty} (g_s - \langle g_s(t) \rangle) h_g(g_s, t) P(g_s, t) dg_s. \end{aligned} \quad (7.6)$$

Approximating $h_g(g_s) \approx h_g(\langle g_s(t) \rangle) + h_g'(\langle g_s(t) \rangle)(g_s - \langle g_s(t) \rangle)$, equation 7.6 becomes

$$\begin{aligned} \frac{d\langle \Delta g_s^2(t) \rangle}{dt} &\approx -\frac{2}{\tau_s} \langle \Delta g_s^2(t) \rangle + q_s^2 \alpha(\langle g_s(t) \rangle, \langle \Delta g_s^2(t) \rangle) \\ &\quad + 2q_s h_g'(\langle g_s(t) \rangle) \cdot \langle \Delta g_s^2(t) \rangle, \end{aligned} \quad (7.7)$$

which has a steady state

$$\langle \Delta g_s^2 \rangle = \frac{1}{2} \frac{q_s^2 \alpha(\langle g_s \rangle, \langle \Delta g_s^2 \rangle)}{\frac{1}{\tau} - q_s h'_g(\langle g_s \rangle)}. \tag{7.8}$$

Thus, the mean+variance-adaptation theory consistency relation for the adapted equilibrium firing rate, α^* , reads

$$\alpha^* = h_g(q_s \tau_s \alpha^*) + \frac{1}{4} h''_g(q_s \tau_s \alpha^*) \left[\frac{q_s^2 \alpha^*}{\frac{1}{\tau} - q_s h'_g(q_s \tau_s \alpha^*)} \right]. \tag{7.9}$$

Higher-order moment theories can be derived by keeping higher terms in the expansions in equations 7.5 and 7.7, and computing the necessary equations for the time evolution of higher statistical moments from the master equation 7.1.

7.1 Validity of Mean-Adaptation Theories. In this section we give a heuristic criterion for the validity of mean-adaptation theories in the static case, and the improved accuracy of the mean+variance-adaptation theory is demonstrated by a numerical example. It is illustrative to first investigate the exactly solvable leaky integrate-and-fire neuron driven by white noise for the parameters considered in La Camera et al. (2004), and subsequently contrast the findings to the 5DF model defined by equations 3.13 to 3.15.

It can be seen by inspection of equation 7.9 that if $h''_g(g_s) \approx 0$ over the regime where $P(g_s)$ is appreciably nonzero, then the mean-adaptation consistency relation,

$$\alpha^* = h_g(q_s \tau_s \alpha^*), \tag{7.10}$$

as in La Camera et al. (2004), results.

First, we use the 1DM master equation to verify the mean-adaptation theory for the leaky integrate-and-fire neuron driven by white noise considered in La Camera et al. (2004). The hazard function, $h_g(g_s, t)$, is referred to there as the response function in the presence of noise and has the exact solution,

$$h_g(g_s, t) = \left[\tau \int_{\frac{C V_r - (m - g_s) \tau}{\sigma \sqrt{\tau}}}^{\frac{C \theta - (m - g_s) \tau}{\sigma \sqrt{\tau}}} \sqrt{\pi} e^{x^2} (1 + \operatorname{erf}(x)) dx \right]^{-1}, \tag{7.11}$$

due to Siegert (1951), Ricciardi (1977), and Amit and Tsodyks (1991), where V_r is the reset potential, θ is the threshold, τ is the membrane potential, C is the membrane capacitance, and $\operatorname{erf}(x) = (2/\sqrt{\pi}) \int_0^x e^{-t^2} dt$ is the error

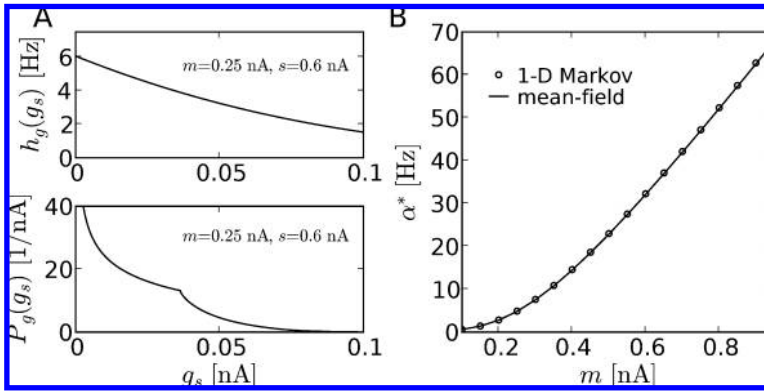


Figure 8: (A, top) The hazard function, $h_g(g_s)$, and (A, bottom) the equilibrium distribution of adaptation states, $P(g_s)$, in the low-firing rate regime ($\alpha^* = 4.83$ Hz, mean current input $m = 0.25$ nA and noise $\sigma = s \cdot \sqrt{2}$ ms with $s = 0.6$ nA) of the leaky integrate-and-fire neuron (LIF) used in La Camera et al. (2004). $P(g_s)$ was determined by numerical solution of the 1DM master equation using the hazard function given in equation 7.11. Neuron parameters: $C = 0.5$ nF, $\tau_m = 20$ ms, $\theta = 20$ mV, $V_r = 10$ mV. Adaptation parameters: $\tau_s = 110$ ms, $q_s \cdot \tau_s = 4$ pA \cdot s. For comparison, the neuron and adaptation parameters are as for Figure 1a in La Camera et al. (2004), except $\tau_r = 0$ ms and $\tau_s = 110$ ms. For the definition of the 1DM model, see Table 1. The hazard function is nearly linear over the distribution of states; thus, terms depending on the variance of $P(g_s)$ in equation 7.9 can be neglected, and mean-adaptation theories will yield good approximations to the adapted ensemble firing rate. (B) The adapted ensemble firing rate, α^* , for a range of mean current inputs, m , determined by numerical solution of the 1DM master equation (circles), and the mean-adaptation theory consistency relation (solid line).

function. As in La Camera et al. (2004), m and σ are the mean and standard deviation of the input current. Upon firing, the adaptation current, g_s , makes a jump of q_s and relaxes with a time constant τ_s . As can be seen in Figure 8A, $h_g(g_s)$ is quite near linear over the regime where $P(g_s)$ is appreciably nonzero, and predictions of the adapted firing rate due to a mean-adaptation theory are in excellent agreement with the 1DM master equation as shown in Figure 8B. The mean+variance-adaptation theory helps us to understand this: agreement is good because $h_g'(g_s) \approx 0$ over the regime where $P(g_s)$ is appreciably nonzero for all firing rates considered.

For the 5DF models defined by equations 3.13 to 3.15, we have $h_g(g_s) \approx a \cdot \exp(-bg_s)$. As can be seen in Figure 9A, $h_g(g_s)$ has an appreciable second derivative over $P(g_s)$, and thus we expect mean-adaptation equilibrium ensemble firing rate predictions to deviate from the ensemble firing rate of the 1DM master equation. Indeed, such deviations are observed and are

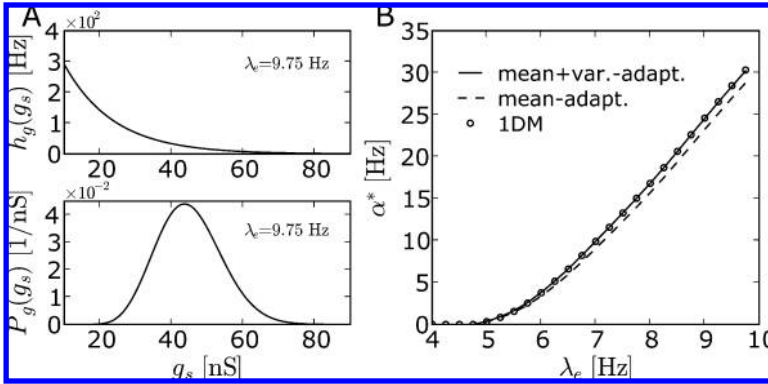


Figure 9: (A, top) The hazard function, $h_g(g_s)$, and (A, bottom) the equilibrium distribution of adaptation states, $P(g_s)$, determined by numerical solution of the 1DM master equation. The hazard function, $h_g(g_s)$, was determined by fitting to 5DF Monte Carlo as in Figure 1 with $\lambda_e = 9.75$ Hz, $\lambda_i = 11.4$ Hz. For the definition of the 5DF and 1DM model, see Table 1. The hazard function has nonzero curvature ($h_g''(g_s) > 0$) over the distribution of states; thus, terms depending on the variance of $P(g_s)$ in equation 7.9 cannot be neglected, and mean-adaptation theory predictions for the adapted ensemble firing rate are expected to be in error. (B) The adapted ensemble firing rate, α^* , for a range of Poisson input rates, λ_e , determined by solution of the 1DM master equation (circles), the mean-adaptation theory consistency relation (dashed line), and the mean+variance-adaptation consistency relation (solid line). As expected, mean-adaptation theory predictions for the adapted firing rate are corrected by the mean+variance-adaptation theory consistency relation in equation 7.9.

corrected by the mean+variance-adaptation consistency relation, as seen in Figure 9B. Thus, a heuristic condition for the validity of mean-adaptation theories is that we must have $h_g''(g_s) \approx 0$ over the regime where $P(g_s)$ is appreciably nonzero. Less heuristically, the contributions due to the second term (and all neglected higher-order terms) on the right-hand side of equation 7.9 must vanish compared to the first. When this condition is violated, higher-order moment theories such as the mean+variance-adaptation theory given here, or the 1DM master equation, should be applied to determine the ensemble firing rate.

For the neuron models considered here, the accuracy of the mean+variance-adaptation theory was also verified in the dynamic case for an OU stimulus as in Figure 7, as shown in Figure 10.

8 Discussion

In this letter, we propose a one-dimensional Markov process (the 1DM model) for modeling neural ensemble activity and spike train statistics

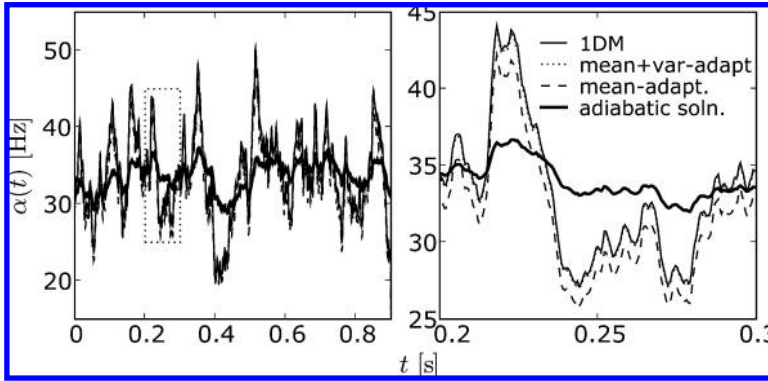


Figure 10: (A) The ensemble firing rate, $\alpha(t)$, in response to an Ornstein-Uhlenbeck process stimulus (as for Figure 7), determined by the 1DM model (solid line), the adiabatic solution (thick solid line) computed by the mean+variance-adaptation consistency relation equation 7.9, the dynamic mean+variance-adaptation theory equations 7.4 to 7.6 (dotted line), and the dynamic mean-adaptation theory equations (dashed line). (B) The region outlined by the dashed rectangle is enlarged, showing consistency between the 1DM model and the mean+variance-adaptation theory, while predictions due to the mean-adaptation theory are poor. For the definition of the 1DM model, see Table 1.

that goes beyond renewal theory by accounting for interspike interval (ISI) correlations due to spike-frequency adaptation (SFA) mechanisms without the need to model the high-dimensional space of the microscopic neuronal state variables.

We demonstrated that the full five-dimensional master equation of a conductance-based integrate-and-fire neuron with SFA and a refractory mechanism driven by Poisson spike trains (the 5DF model) can be reduced to a two-dimensional master equation plus filtering differential equations accounting for synaptic dynamics (the 2DM model), under an adiabatic elimination of the fast variables v , g_e , g_i , assuming the neuron has nonzero synaptic time constants and is in the high-conductance state. The resulting 2DM master equation is a two-dimensional generalization of the Markov process proposed at the outset as an extension of renewal theory to account for ISI correlations.

We presented methods for generating inhomogeneous realizations of the proposed 1DM and 2DM models and a method for solving their master equations numerically. The 2DM model was shown to accurately predict firing rate profiles of the full system under dynamic stimulation and conditional ISI distributions and serial ISI correlations under static stimulation.

It was shown that mean-adaptation theories for spike-frequency adapting neurons with noisy inputs such as in La Camera et al. (2004) and higher-order statistical moment theories can be derived from the 1DM master equation as long as one neglects the refractory period. A heuristic condition for the validity of mean-adaptation theories was derived and found to be violated for the neuron model (5DF) and parameters considered here. Furthermore, a mean+variance-adaptation theory was derived that corrected the ensemble firing rate predictions of mean-adaptation theories in this case.

8.1 Comparison with Other Studies of Adaptation. Studies of the firing rates of networks and ensembles of spike-frequency adapting neurons due to Latham et al. (2000) and Fuhrmann et al. (2002) augment a Wilson and Cowan equation (Wilson & Cowan, 1972) for the firing rate with a mean adaptation variable.

As is typical of the Wilson and Cowan approach, the ensemble firing rate, α , enters a differential equation of the form

$$\tau_e \frac{d\alpha}{dt} = -\alpha + h_g(\langle g_s(t) \rangle, \dots), \quad (8.1)$$

where $h_g(\langle g_s(t) \rangle, \dots)$ is the static firing rate given the input and the mean adaptation, and τ_e is the timescale for relaxation to a firing rate equilibrium. As is suggested in Fuhrmann et al. (2002), τ_e is determined mainly by the membrane time constant of the neuron, but is also affected by the mean amplitude of the input, and is treated there as a free parameter.

It has been argued in Gerstner (2000), Brunel, Chance, Fourcaud, and Abbott (2001), Fourcaud and Brunel (2002), Renart et al. (2004), and La Camera et al. (2004) that for current and conductance-based synapses with nonzero time constants and biological input statistics, the ensemble firing rate responds instantaneously to input currents, and synaptic filtering dominates. In this case, the Wilson and Cowan equation for α can be replaced by an instantaneous f-I function, and the synaptic currents or conductances modeled by relaxation equations for their means and variances. This is the approach taken in La Camera et al. (2004). Thus, one sidesteps the concerns mentioned in Fuhrmann et al. (2002) that the Wilson and Cowan equation “cannot be rigorously derived from the detailed integrate-and-fire model” and has been “shown not to accurately describe the firing rate dynamics [by] (Gerstner, 2000).”

The models due to Latham et al. (2000), Fuhrmann et al. (2002), and La Camera et al. (2004) all approximate the evolution of the ensemble of adaptation variables by its mean value and are therefore mean-adaptation theories. La Camera et al. (2004) state that such mean-adaptation theories are a good approximation under the assumption that “adaptation is slow compared to the timescale of the neural dynamics. In such a case, the

feedback [adaptation] current . . . is a slowly fluctuating variable and does not affect the value of s [the standard deviation of the input current]."

La Camera et al. (2004) explore adaptation time constants on the order of 100 ms under the assumption that the adaptation dynamics are "typically slower than the average ISI." They report that "for irregular spike trains the agreement is remarkable also at very low frequencies, where the condition that the average ISI be smaller than τ_N [the time constant of adaptation] is violated. This may be explained by the fact that although $\langle ISI \rangle > \tau_N$, the ISI distribution is skewed towards smaller values, and [the mean adaptation current proportional to the firing rate] . . . is still a good approximation."

In section 7 we used the 1DM master equation to derive a mean+variance-adaptation theory, the next correction to the mean-adaptation theories in La Camera et al. (2004), yielding another explanation for the success reported there. We found that the error in the firing rate in La Camera et al. remained small because the hazard function used there is a nearly linear function of the adaptation variable in the interesting regime where $P(g_s)$ is appreciably nonzero. Thus, perturbing contributions to the average firing rate from deviations of the adaptation variable above and below the mean over the course of one ISI roughly cancel on average. For the neuron model (5DF) and parameters considered here, the hazard function has an appreciable nonlinearity resulting in erroneous predictions of the firing rate when using a mean-adaptation theory. The mean+variance-adaptation theory derived here corrected the predictions.

It is appropriate to reiterate that both the 1DM master equation and the resulting mean+variance-adaptation theory approximation considered here neglect refractory dynamics. It was demonstrated by the adiabatic reduction of the 5DF model to the 2DM model that the inclusion of a relative refractory period requires a two-dimensional master equation. Indeed, as shown in Figure 6, oscillations emerge for large and fast stimulation changes that are qualitatively captured by the 2DM model but not by the 1DM model. It remains to be seen if a two-dimensional mean- or mean+variance-adaptation theory can be constructed that accounts for this behavior, and under what conditions it can be reduced to a one-dimensional model by simply rescaling the firing rate by $f' = 1/(1/f + \tau_{\text{eff}})$, as in La Camera et al. (2004) for the absolute refractory period case, where τ_{eff} is some effective absolute refractory period of the relative refractory mechanism.

In Benda and Herz (2003), a thorough mathematical analysis of several well-known mechanisms for SFA based on biophysical kinetics is performed for the case of a suprathreshold current. A universal phenomenological mean-adaptation model for such biophysical mechanisms for SFA is introduced with much the same form as later used in La Camera et al. (2004) for the case of noisy drive. Methods are given to completely parameterize the model using quantities that can be easily measured by standard recording techniques. Implications for signal processing are considered there and in subsequent publications (Benda, Longtin, & Maler, 2005).

In Chacron et al. (2003), a novel approach is taken compared to Latham et al. (2000), Fuhrmann et al. (2002), Benda and Herz (2003), and La Camera et al. (2004). There an expression is derived for the serial correlation coefficient of ISIs in the static case by employing a Markov chain. In their analysis, they define a quantity analogous to the static distribution $P^\dagger(t_s)$ here. In their framework, they prove that adaptation of the threshold fatigue form used there results in ISI correlations as have been observed experimentally (Longtin & Racicot, 1997; Chacron et al., 2000; Nawrot et al., 2007). Their expression, however, contains integrals that require “the computation of the FPT [first-passage time] PDF of the Ornstein-Uhlenbeck process through an exponential boundary. Given that no general analytical expression is available for this quantity, derivation of the correlation from the integrals can be computationally more demanding than estimating the same quantities from simulations” (Chacron et al., 2003). Subsequently, only simulations are performed, and the derived expression is never compared to the simulated result. Thus, they miss an important benchmark to ensure the calculations are correct. It is possible that the numerical techniques used here could be applied to compute a prediction for the correlation coefficient by the expression they derive and subsequently compared to the simulated result.

Mean-adaptation theories cannot be used to model the correlation between subsequent ISIs, as they do not preserve the ensemble statistics. Our approach is that one simply not replace the trajectory of the adaptation variable, g_s , by its mean. This resolves the problem in the development in La Camera et al. (2004) that the mean input current and instantaneous g_s have an equal role in determining the instantaneous firing rate, and g_s cannot be consistently replaced by its mean. What results is the 1DM master equation presented here. We subsequently calculate an expression for the inhomogeneous conditional ISI distribution and compare it to 5DF Monte Carlo in the static case. Furthermore, we calculate the variation of the mean of the conditional ISI distribution as a function of the preceding ISI, a generalization of the serial correlation coefficient of ISIs, and compare it to 5DF Monte Carlo. By our Markov process master equation, we avoid the difficulty encountered in Chacron et al. (2003) of treating the first passage times of an Ornstein-Uhlenbeck process through an exponential boundary, while capturing the full inhomogeneous ensemble dynamics in a framework that is tractable.

8.2 On the Adiabatic Reduction of the Master Equation. Under the assumption that the neuron is in the high-conductance state due to biologically realistic noisy inputs, we show that the 5DF master equation for the conductance-based spike frequency adapting relative refractory integrate-and-fire neuron model used here can be reduced to the 2DM master equation by an adiabatic elimination of fast variables. The variables that remain are those of SFA and the relative refractory mechanism, and the form is

analogous to the 1DM master equation proposed to extend renewal theory to a class of Markov processes that account for SFA.

The adiabatic reduction does not solve explicitly the firing rate of the given neuron model (without adaptation or the refractory mechanism) or rely on such a solution. We leave the firing rate dynamics of the given neuron model (without adaptation or the refractory mechanism) encapsulated in the hazard function (see equation 3.23). The approach applies to other models of adaptation such as the adapting threshold models in Chacron et al. (2003) and the current-based adaptation models in La Camera et al. (2004).

Concerning the generality of the adiabatic elimination for the adaptation variable, we expect it could be applied to a larger class of formally spiking neuron models with fast, intrinsic dynamics compared to adaptation. For those interested in modeling a class of neurons where a solution to equation 3.23 already exists, the framework can be easily and immediately applied. The fitting methods presented allow the connection to be made between models for which an explicit solution for the hazard function is unknown and the 1DM and 2DM models presented here. What results is a reduced state space to explore for functional implications.

The generality of treating the relative refractory mechanism as a slow variable in the adiabatic elimination is less clear. There are some issues that need to be clarified before one could specify the class of neurons to which it applies. Specifically, the relationship between the requirement that the neuron be in the high-conductance state (small effective τ_m) and the requirement that the synapses have nonvanishing time constants ($\tau_e > 0$) resulting in a nonvanishing probability at threshold ($P(v_{th}, \dots) > 0$) remains to be thoroughly investigated. The delta-conductance-based approach in Meffin et al. (2004), for example, does not satisfy the second requirement. The nonvanishing probability at threshold seems to be a criterion for the neuron to respond quickly to the synaptic signal (Fourcaud & Brunel, 2002; Renart et al., 2004).

An important step in the reduction is the treatment of the synaptic conductances. As their statistics are assumed to instantaneously determine the equilibrium statistics of the membrane potential, they were removed from the master equation. Then differential equations were found for their first statistical moments (means) in terms of the rate of the Poisson process input, as in La Camera et al. (2004). One weakness of the fitting approach used here is that we cannot account for the dynamics of the second central moment (variance), as was done in La Camera et al., and modeling both dynamic excitation and inhibition simultaneously requires a laborious fitting of a two-dimensional space of synaptic inputs. Further work will apply methods such as those due to Moreno-Bote and Parga (2004) to obtain a solution to equation 3.23 without fitting, thus allowing ensemble studies of adapting network models and analysis as in Latham et al. (2000) with the rigor of, for example, (Brunel, 2000), and the possibility for quantitative agreement with traditional large-scale network simulations.

8.3 Beyond Renewal Theory. We reviewed standard results of inhomogeneous renewal theory in appendix C and uncovered a conceptual error often made in the literature when using the intensity-rescaling transformation to make the transition from homogeneous (static) to inhomogeneous (dynamic) renewal theory. We clarified and remedied the problem by presenting a correct renewal process generation scheme as discussed in Devroye (1986).

By means of a variable transformation, we provided a link between the 1DM model and inhomogeneous renewal theory methods, allowing direct comparison and contrast. The 1DM master equation was found to have an analogous structure to the renewal master equation, but with a state space spanning the whole real line. Furthermore, the 1DM state is not reborn to a universal initial value upon spiking, as in renewal theory (zero age), but reinserted to a state that is a function of the state just prior to spiking. This fact introduces a memory into the system and results in negative ISI correlations as reported in Chacron et al. (2003).

Due to the detailed adiabatic reduction and fitting, we proposed the nested exponential form of the hazard function as given by equation 2.10 and the state-dependent reinsertion function as given by equation 2.7 for the conductance-based SFA mechanism considered here. The hazard function (perhaps time-dependent) and the reinsertion function together are a complete specification of the proposed Markov model given an initial distribution of states. We provided a numerical recipe to efficiently generate inhomogeneous realizations of the proposed Markov process.

With an additional dimension for a relative refractory mechanism, the Markov process faithfully reproduces the transient dynamics and ISI correlations of 5DF Monte Carlo, as expected by the adiabatic reduction. The same comparison between a one-dimensional Markov process and a neuron model without the relative refractory mechanism was not done, as we found that without refractory mechanisms, the neuron model used exhibited a high probability to spike just after spiking due to correlations in the synaptic conductance on the timescale of the refractory mechanism. We feel this is a bug rather than a feature of neuron models without a refractory mechanism. Thus we chose not to build a Markov process to account for it. Furthermore, the proposed relative refractory mechanism requires only slightly more effort than treating an absolute refractory period, as done in Nykamp and Tranchina (2001). When the hazard function calibrated for the 2DM model is used directly for the 1DM model, reasonable agreement to refractory neuron models was still observed for the moderate firing rates considered.

8.4 Suprathreshold Stimuli. For large and rapid changes in stimulus that bring the ensemble predominantly into the suprathreshold regime, the predictions due to numerical solutions of the 2DM model deviated somewhat from 5DF Monte Carlo simulations, as seen in Figure 6. The reasons

for this are twofold. First, the stimulus brings us into a regime where the exponential fitting procedure for $h(t_s, t_r)$ begins to fail and was poorly populated with data points. This fact likely accounts for the larger amplitude of the oscillations of the 2DM model compared to 5DF Monte Carlo. It is likely that a choice of function that improves the fit in this regime or a proper analytical solution for $h(t_s, t_r)$ would improve the agreement here. Second, following the large stimulus change, a large portion of the population is in the suprathreshold regime where neurons make large migrations from the reset potential directly to the threshold following a spike. The 2DM model completely neglects the dynamics of the membrane potential and thus this migration period, resulting in the phase lead over the full system.

A closer inspection of Figure 6 reveals a transition from predominantly supra- to predominantly subthreshold firing. Shortly after stimulus onset, a large portion of the population fires almost immediately and is reinserted with the adaptation conductance increased by q_s , that is, a mass exodus in phase space. For the 2D case, the neurons also start a refractory period upon reinsertion; in the 1D case, they do not. The stimulus is sufficiently strong that in the 2D case, it is still suprathreshold following the refractory period. In the 1D case, there is no refractory period, and the neurons can fire immediately following a spike cycle, and no lull is seen in the firing rate following the initial mass exodus. For the 2D case, and even the renewal case, the system is refractory following the mass exodus, and a lull in the firing rate results, to peak again as the neurons are released from the refractory state. With the accumulation of adaptation, the fraction of the ensemble participating in subsequent exodus events is ever diminished as more and more neurons enter the subthreshold regime where neurons survive for highly variable durations following the refractory period. Thus, for large stimuli that keep the neuron suprathreshold over several spikes, the population is initially synchronized, firing at a rate determined by the refractory mechanism. As adaptation accumulates, spiking becomes more irregular, and the neurons desynchronize.

The desynchronization of neurons driven by suprathreshold current has been observed experimentally in Mainen and Sejnowski (1995). It is shown there that this transition to the subthreshold regime due to adaptation is not strictly necessary for the neurons to desynchronize due to the constant presence of noise. However, adaptation is also a mechanism by which an otherwise irregularly firing neural ensemble is synchronized at a stimulus onset. Following such a synchronization, the transition from the predominantly suprathreshold regime to the predominantly subthreshold regime induced by the accumulation of adaptation is akin to a transition from a noisy oscillator firing mode to a point process firing mode. While the ensemble would gradually desynchronize in the noisy oscillator firing mode, the transition to the point process firing mode over only a few spikes ensures this occurs much more rapidly. Thus, adaptation works to both synchronize and then desynchronize at changes in stimulus. This is an implementation of novelty

detection and is related to the high-pass filtering properties of SFA reported in Benda et al. (2005). Evidence for a synchronization-desynchronization coding scheme for natural communication signals was recently reported for the spike-frequency adapting P-unit electroreceptors of weakly electric fish in Benda, Longtin, and Maler (2006).

9 Conclusion

In this letter, we have focused on establishing a framework for rigorously treating the dynamic effects of spike-frequency adaptation and refractory mechanisms on neural ensemble spiking. The resulting master equation formalism unifies renewal theory models and previous studies on adaptation (e.g., Latham et al., 2000; Fuhrmann et al., 2002; Chacron et al., 2003; Benda & Herz, 2003; La Camera et al., 2004) into an ensemble, or population density framework such as those due to Knight (1972, 2000), Brunel (2000), Omurtag et al. (2000), Nykamp and Tranchina (2000), Fourcaud and Brunel (2002), Richardson (2004), Rudolph and Destexhe (2005), Meffin et al. (2004), and Moreno-Bote and Parga (2004). The resulting methods are new and powerful tools for accurately modeling spike-frequency adaptation, an aspect of neuron dynamics ubiquitous in excitatory neurons that has been largely ignored in neural ensemble studies thus far due to the added difficulties of treating the extra state variable.

By distilling the detailed neuron model down to two essential dimensions, spike-frequency adaptation and a relative refractory period, using an adiabatic elimination, their central role in perturbing neural firing is emphasized. Future work will employ the framework to examine the functional implications of spike-frequency adaptation. Given the variety of intriguing and prominent consequences such as interspike interval correlations and transient synchronization following stimulus changes, one is compelled to question if spike-frequency adaptation can be neglected when considering, for example, the dynamic nature of the neural code (Shadlen & Newsome, 1998; Rieke, Warland, de Ruyter van Steveninck, & Bialek, 1997), the propagation of synchrony (Abeles, 1991; Diesmann, Gewaltig, & Aertsen 1999), or the function of spike-timing-based learning rules (Gerstner, Kempter, van Hemmen, & Wagner, 1996; Song, Miller, & Abbott, 2000).

Appendix A: Neuron and Adaptation Model Parameters

The parameters of the 5DF neuron model given in equations 3.13 to 3.15 were determined by fitting to a single-compartment Hodgkin-Huxley (HH) model of a pyramidal neuron under various conditions using NEURON (Hines & Carnevale, 1997) as described in Muller (2003). The HH model and parameters are taken from Destexhe, Contreras, and Steriade (1998).

The phenomenological mechanism for spike-frequency adaptation (SFA) used here, the counterpart to the M-current and AHP-current mechanisms

in the HH model, was inspired by (Dayan & Abbott, 2001), and similar models have been proposed in (Koch, 1999) and Fuhrmann et al. (2002), and more recently generalized in Brette and Gerstner (2005).

Additionally, a relative refractory period (RELREF) mechanism identical to the SFA mechanism was added, but with a much shorter time constant and a much larger conductance increase. Both the SFA and RELREF mechanisms consist of an action potential (AP) activated and exponentially decaying conductance coupled to an inhibiting reversal potential so that the standard membrane equation takes the form:

$$c_m \frac{dv(t)}{dt} = g_l(E_l - v(t)) + g_e(t)(E_e - v(t)) + g_i(t)(E_i - v(t)) \\ + g_s(t)(E_s - v(t)) + g_r(t)(E_r - v(t)).$$

If v exceeds the threshold v_{th} :

- v is reset to v_{reset} .
- $g_s \mapsto g_s + q_s$.
- $g_r \mapsto g_r + q_r$.
- The time of threshold crossing is added to the list of spike times.

All conductances, $g_x(t)$, where $x \in \{s, r, e, i\}$ are governed by an equation of the form

$$\frac{dg_x(t)}{dt} = -\frac{1}{\tau_x} g_x(t).$$

The arrival of a spike at a synapse triggers $g_x \mapsto g_x + q_x$ for $x \in \{e, i\}$. Poisson processes were used to supply spike trains to the 1000 excitatory and 250 inhibitory synapses, where Poisson rates in the range 3 to 20 Hz were used as described in the text for each specific simulation. The synaptic model and parameters were directly transferred from the HH models, while the remaining parameters, as determined by fits to the HH model, are given in Table 3.

Appendix B: Further Details on the Adiabatic Reduction ---

In this appendix, we give the mathematical steps that lead from equation 3.16 to 3.20 in a more detailed way.

For notational simplicity, we introduce the five-dimensional state variable $x = (v, g_e, g_i, g_s, g_r)$. The indices 1, 2, 3, 4, 5 shall correspond to v, e, i, s, r , as used in the definition of the neuron model in equations 3.13 to 3.15 (e.g., $\tau_2 := \tau_e$). The partial derivatives with respect to x_μ are denoted by ∂_μ and with respect to time by ∂_t . Furthermore, we define $P(x_1, x_2, x_3, x_4, x_5) = 0$ if one or more of the conductances x_2, \dots, x_5 is negative.

Table 3: Neuron and Synapse Model Parameters Used for Simulations of the Full System (5DF) Given by Equations 3.13 to 3.15.

Parameter	Description	Value
v_{th}	Threshold voltage	-57 mV
v_{reset}	Reset voltage	-70 mV
c_m	Membrane capacitance	289.5 pF
g_l	Membrane leak conductance	28.95 nS
E_l	Membrane reversal potential	-70 mV
q_r	RELREF quantal conductance increase	3214 nS
τ_r	RELREF conductance decay time	1.97 ms
E_r	RELREF reversal potential	-70 mV
q_s	SFA quantal conductance increase	14.48 nS
τ_s	SFA conductance decay time	110 ms
E_s	SFA reversal potential	-70 mV
$E_{e,i}$	Reversal potential of excitatory and inhibitory synapses, respectively	0 mV, -75 mV
$q_{e,i}$	Excitatory and inhibitory synaptic quantal conductance increase	2 nS
$\tau_{e,i}$	Excitatory and inhibitory synaptic decay time	1.5 ms, 10.0 ms

The master equation governing the evolution of the probability density $P(x, t)$ may be formulated as a conservation equation:

$$\partial_t P(x, t) = -\text{div} J(x, t) + \delta(x_1 - v_{\text{reset}}) J_1(v_{\text{th}}, x_2, x_3, x_4 - q_4, x_5 - q_5, t). \quad (\text{B.1})$$

The second term on the right-hand side of equation B.1 accounts for neurons that cross the threshold surface $x_1 = v_{\text{th}}$ at time t with the state variables $(v_{\text{th}}, x_2, x_3, x_4 - q_4, x_5 - q_5)$ and are reinserted to $(v_r, x_2, x_3, x_4, x_5)$.

The probability current $J(x, t)$ is determined by the underlying stochastic differential equations 3.13 to 3.15. The components $J_\mu(x, t)$ for $\mu = 1, \dots, 5$ consist of the current due to the drift terms, $\beta_\mu(x)$, and for $\mu = 2, 3$ of additional currents due to the excitatory and inhibitory input Poisson spike trains, respectively. The drift term for the membrane potential reads

$$\beta_1(x) := \frac{1}{c_m} \left(\sum_{\mu=2}^5 x_\mu (E_\mu - x_1) + g_l (E_l - x_1) \right). \quad (\text{B.2})$$

For the conductances x_μ with $\mu = 2, \dots, 5$, the drift terms are:

$$\beta_\mu(x) = \beta_\mu(x_\mu) := -\frac{1}{\tau_\mu} x_\mu. \quad (\text{B.3})$$

The components of the probability current for $\mu = 1, 4, 5$ obey the equation

$$J_\mu(x, t) = \beta_\mu(x)P(x, t). \quad (\text{B.4})$$

For the excitatory synaptic conductance x_2 , the component $J_2(x, t)$ is

$$\begin{aligned} J_2(x, t) &= \beta_2(x)P(x, t) \\ &+ \int_0^{x_2} \left[\int_0^\infty W_2(y_2, y_1, t)P(x_1, y_1, x_3, \dots, x_5)dy_2 \right] dy_1 \\ &- \int_0^{x_2} \left[\int_0^\infty W_2(y_1, y_2, t)P(x_1, y_2, x_3, \dots, x_5)dy_2 \right] dy_1. \end{aligned} \quad (\text{B.5})$$

The component $J_3(x, t)$ has a similar form with obvious modifications. Since the synaptic input is modeled as a Poisson process, the transition rates $W_\mu(y_1, y_2, t)$ for $\mu = 2, 3$ may be written as

$$W_\mu(y_1, y_2, t) = \nu_\mu(t)\delta(y_1 - (y_2 + q_\mu)), \quad (\text{B.6})$$

given the presynaptic firing rates $\nu_\mu(t)$. The diffusion approximation can be obtained by a Kramers-Moyal expansion of the components J_2 and J_3 (Gardiner, 1985).

B.1 Integration. To obtain an equation for the marginal probability distribution, $P(x_4, x_5, t)$, one integrates equation B.1 over x_1, x_2, x_3 . The integral of the terms $\partial_\mu J_\mu(x, t)$ on the right-hand side in B.1 for $\mu = 2, 3$ vanishes due to the boundary condition that the probability current vanishes in the limit $x_\mu \rightarrow 0$ and $x_\mu \rightarrow \infty$ for $\mu = 2, 3$:

$$\int_0^\infty \partial_\mu J_\mu(x, t)dx_\mu = \lim_{x_\mu \rightarrow \infty} J_\mu(x, t) - J_\mu(x, t)\Big|_{x_\mu=0} = 0. \quad (\text{B.7})$$

The component $J_1(x, t)$ yields a nonvanishing contribution:

$$\begin{aligned} &\int_0^\infty \int_0^\infty \left(\int_{-\infty}^{v_{\text{th}}} \partial_1 J_1(x, t)dx_1 \right) dx_2 dx_3 \\ &= \int_0^\infty \int_0^\infty J_1(v_{\text{th}}, x_2, \dots, x_5, t)dx_2 dx_3. \end{aligned} \quad (\text{B.8})$$

The reinsertion term involves an integration over a delta distribution:

$$\begin{aligned} &\int_0^\infty \int_0^\infty \left(\int_{-\infty}^{v_{\text{th}}} \delta(x_1 - v_{\text{reset}})J_1(v_{\text{th}}, x_2, x_3, x_4 - q_4, x_5 - q_5, t)dx_1 \right) dx_2 dx_3 \\ &= \int_0^\infty \int_0^\infty J_1(v_{\text{th}}, x_2, x_3, x_4 - q_4, x_5 - q_5, t)dx_2 dx_3. \end{aligned} \quad (\text{B.9})$$

Integration of the left-hand side in equation B.1 results in:

$$\int_0^\infty \int_0^\infty \int_{-\infty}^{v_{\text{th}}} (\partial_t P(x, t)) dx_1 dx_2 dx_3 = \partial_t P(x_4, x_5, t). \quad (\text{B.10})$$

Plugging these results into equation 3.16 yields:

$$\begin{aligned} \partial_t P(x_4, x_5, t) = & - \sum_{\mu=4,5} \partial_\mu (\beta_\mu(x_\mu) P(x_4, x_5, t)) \\ & + \int_0^\infty \int_0^\infty J_1(v_{\text{th}}, x_2, x_3, x_4 - q_4, x_5 - q_5, t) dx_2 dx_3 \\ & - \int_0^\infty \int_0^\infty J_1(v_{\text{th}}, x_2, \dots, x_5) dx_2 dx_3. \end{aligned} \quad (\text{B.11})$$

Returning to the initial notation and using the definition for $J_1(x, t) = \beta_1(x, t)P(x, t)$ yields equation 3.20.

Appendix C: Inhomogeneous Renewal Processes

The proposed Markov models can be easily understood by analogy to inhomogeneous renewal theory. We review some standard results thereof, which define the renewal models used in the text.

Poisson and gamma renewal processes, both special cases of a renewal process, are used extensively to model the spike train statistics of cortical neurons (van Rossum, Bi, & Turrigiano, 2000; Song & Abbott, 2001; Rudolph & Destexhe, 2003b; Shelley et al., 2002), and are treated in detail in (Gerstner & Kistler, 2002) in sections 5.2, 5.3, 6.2.2, and 6.3.2. While the treatment in section 6.2.2 is developed for spike response model neurons with escape noise and in section 6.3.2 for populations of neurons satisfying a few basic assumptions, it is not explicitly stated there that the analysis is that of an arbitrary inhomogeneous renewal process, though it is mentioned in Gerstner (2001). We first reiterate this fact by producing the main results of section 6.2.2 and 6.3.2 of Gerstner and Kistler (2002) using an inhomogeneous generalization of the notation of Cox (1962), a classic reference work on homogeneous renewal theory. Second, we present a recipe for efficiently generating spike trains of a general inhomogeneous renewal process.

In what follows, by working exclusively with the inhomogeneous hazard function, we avoid the pitfall of studies that erroneously assume an intensity-rescaling transformation of a stationary gamma renewal process

with parameter γ , or a yields an inhomogeneous gamma renewal process with parameter γ , or a (Barbieri, Quirk, Frank, Wilson, & Brown, 2001; Gazères, Borg-Graham, & Frégnac, 1998).

A renewal process is defined here to be *inhomogeneous* when its hazard function takes the form $\rho(\tau, t)$, where τ denotes the age, and t denotes the explicit dependence of the hazard function on time. The ensemble firing rate³ at t , denoted by $\alpha(t)$, is the expectation value,

$$\alpha(t) = \langle \rho(t) \rangle = \int_0^\infty \rho(s, t) f^-(s, t) ds, \quad (\text{C.1})$$

where $f^-(\tau, t)$ denotes the probability density function (PDF) of times since last renewal, also called the backward recurrence time in Cox (1962). The PDF, $f^-(\tau, t)$, can be determined by reasoning that the probability that the system has an age in the interval $(\tau, \tau + \Delta\tau)$ is equal to the probability that there is a renewal in the time interval $(t - \tau, t - \tau + \Delta\tau)$ and that the system subsequently survives until t . This yields

$$f^-(\tau, t) = \alpha(t - \tau) \mathcal{F}(\tau, t - \tau), \quad (\text{C.2})$$

where $\mathcal{F}(\Delta t, t)$ is the inhomogeneous survival function, representing the probability that the system will survive for a time Δt after t . Generalizing equation 1.2.10 in Cox (1962) for the inhomogeneous case, we have

$$\mathcal{F}(\Delta t, t) = \exp\left(-\int_0^{\Delta t} \rho(s, t + s) ds\right). \quad (\text{C.3})$$

Plugging equation C.2 into C.1 results in the equivalent of equations 6.44 and 6.45 of Gerstner and Kistler (2002).

A differential formulation of equations C.1 to C.3 is possible. First, note that age increases with increasing t and thus

$$\frac{d\tau}{dt} = 1.$$

This suggests a transform of the age variable $\tau \rightarrow \tau' = t - \tau$, as in equation 6.46 of Gerstner and Kistler (2002). This new age variable, τ' , is stationary with the evolution of t . We define the stationary backward recurrence time PDF as

$$f_s^-(\tau', t) := f^-(t - \tau', t).$$

³The ensemble firing rate is referred to as the population activity, $A(t)$, in Gerstner and Kistler, 2002.

Thus,

$$\begin{aligned} \frac{d}{d\tau} f_s^-(\tau', t) &= \frac{\partial}{\partial t} f_s^-(\tau', t) \\ &= \frac{\partial}{\partial t} (\alpha(\tau') \mathcal{F}(t - \tau', \tau')), \end{aligned}$$

and differentiation of equation C.3 yields $\frac{d}{dt} \mathcal{F}(t - \tau', \tau') = \mathcal{F}(t - \tau', \tau') \rho(t - \tau', t)$ whereby we have

$$\begin{aligned} \frac{d}{dt} f_s^-(\tau', t) &= -\alpha(\tau') \mathcal{F}(t - \tau', \tau') \rho(t - \tau', t) \\ \frac{d}{dt} f_s^-(\tau', t) &= -f_s^-(\tau', t) \rho(t - \tau', t). \end{aligned} \tag{C.4}$$

This relation determines $\frac{d}{dt} f_s^-(\tau', t)$ for $\tau' \in (-\infty, t)$. Additionally, we need to ensure that the normalization of $f_s^-(\tau, t)$ is preserved, namely, that

$$\int_{-\infty}^{\infty} \frac{\partial}{\partial t} f_s^-(\tau, t) d\tau = 0. \tag{C.5}$$

Splitting the integral into three regions of interest, we have

$$\begin{aligned} \lim_{\Delta t \rightarrow 0^+} \left[\int_{-\infty}^{t-\Delta t} \frac{\partial}{\partial t} f_s^-(s, t) ds \right. \\ \left. + \int_{t-\Delta t}^{t+\Delta t} \frac{\partial}{\partial t} f_s^-(s, t) ds \right. \\ \left. + \int_{t+\Delta t}^{\infty} \frac{\partial}{\partial t} f_s^-(s, t) ds \right] = 0. \end{aligned}$$

Since $f_s^-(\tau' > t, t) = 0$, the third integral is zero. We then have

$$\lim_{\Delta t \rightarrow 0^+} \int_{t-\Delta t}^{t+\Delta t} \frac{\partial}{\partial t} f_s^-(s, t) ds = - \int_{-\infty}^t \frac{\partial}{\partial t} f_s^-(s, t) ds.$$

Since the contribution from equation C.4 in the integral on the left-hand side is vanishing, we need to add an additional term to $\frac{d}{dt} f_s^-(\tau, t)$, which is zero for all $\tau \neq t$ but which has a finite integral when integrating around t . This can be achieved by addition of a δ -function term:

$$\frac{d}{dt} f_s^-(\tau, t) \rightarrow \frac{d}{dt} f_s^-(\tau, t) - \delta(\tau - t) \int_{-\infty}^t \frac{\partial}{\partial t} f_s^-(s, t) ds.$$

Clearly the factor behind the δ -function is $\alpha(t)$. Thus, we have the final form,

$$\frac{d}{dt} f_s^-(\tau', t) = \begin{cases} -f_s^-(\tau', t)\rho(t - \tau', t), & \tau' < t \\ 0, & \tau' \geq t \end{cases} + \alpha(t)\delta(\tau' - t), \quad (\text{C.6})$$

defined for $\tau' \in (-\infty, \infty)$. Equation C.6 expressed in terms of $f^-(\tau, t)$ results in the master equation,

$$\frac{\partial}{\partial t} f^-(\tau, t) = -\frac{\partial}{\partial \tau} f^-(\tau, t) - f^-(\tau, t)\rho(\tau, t) + \alpha(t)\delta(\tau), \quad (\text{C.7})$$

defined for $\tau \in [0, \infty)$. This is exactly equation 6.43 in Gerstner and Kistler (2002). It is analogous to equation 2.9, but with reinsertion to $\tau = 0$ after a spike.

C.1 Numerical Solution of the Renewal Master Equation. As the renewal master equation C.7 is just a special case of the 1DM master equation, it can be solved with the same numerical techniques as described in section 5.1. The content of the δ term in equation C.7 is that all probability lost due to the death term (the second term on the rhs) is accumulated and reinserted to the $\tau = 0$ bin. Thus, we are spared the complication of treating state-dependent reinsertion of probability, as was necessary for the 1DM and 2DM master equations.

C.2 Generating Random Numbers of a General Hazard Function. Random numbers with a general hazard function can be generated by the thinning method as discussed in Devroye (1986) and summarized here. The maximum of the hazard function, $\rho_{\max} = \max_{\tau, t}(\rho(\tau, t))$, must be known. Sequential event intervals are generated using a homogeneous Poisson process with a rate of ρ_{\max} . The resulting spike train is then sequentially thinned, given the event time t and time since last event τ , by the rule:

1. Generate a uniform random number, T , on $[0, 1)$.
2. if $\rho(\tau, t)/\rho_{\max} > T$, keep the event in the spike train; otherwise remove it.

The remaining event times are consistent with the prescribed hazard function.

For the case of random number generation for a GRP, evaluation of $\rho(\tau, t)$ using equation 4.6 is numerically unstable for large τ and costly. An implementation of the algorithm (Shea, 1988) for calculating the cumulative hazard function of a gamma renewal process is available in `pgamma.c` of the Mathlib of the R statistics environment (Ihaka & Gentleman, 1996)

under the GNU Public License. Alternatively, the logarithm of the function `gsl_sf_gamma_inc_Q` provided by the GNU Scientific Library can be used. The hazard function can then be calculated by a simple discrete difference calculation of the derivative. Time dependence can be introduced by giving a time dependence to the parameters of the gamma distribution.

Acknowledgments

This work is supported in part by the European Union under the grant IST-2005-15879 (FACETS). Thanks to M. Rudolph, A. Destexhe, M. Diesmann, N. Brunel, M. Pospischil and N. Nurpeissov for helpful discussion. Thanks to the reviewers for their many detailed and insightful comments which have had a significant and positive impact on this letter.

References

- Abeles, M. (1991). *Corticonics*. Cambridge: Cambridge University Press.
- Amit, D. J., & Tsodyks, M. V. (1991). Quantitative study of attractor neural network retrieving at low spike rates: I. Substrate-spikes, rates and neuronal gain. *Network*, 2, 259–273.
- Barbieri, R., Quirk, M., Frank, L., Wilson, M., & Brown, E. (2001). Construction and analysis of non-Poissonian stimulus-response models of neural spiking activity. *Journal of Neuroscience Methods*, 105, 25–37.
- Benda, J., & Herz, A. (2003). A universal model for spike-frequency adaptation. *Neural Computation*, 15, 2523–2564.
- Benda, J., Longtin, A., & Maler, L. (2005). Spike-frequency adaptation separates transient communication signals from background oscillations. *Journal of Neuroscience*, 25, 2312–2321.
- Benda, J., Longtin, A., & Maler, L. (2006). A synchronization-desynchronization code for natural communication signals. *Neuron*, 52, 347–358.
- Brette, R., & Gerstner, W. (2005). Adaptive exponential integrate-and-fire model as an effective description of neuronal activity. *Journal of Neurophysiology*, 94, 3637–3642.
- Brunel, N. (2000). Dynamics of sparsely connected networks of excitatory and inhibitory spiking neurons. *Journal of Computational Neuroscience*, 8, 183–208.
- Brunel, N., Chance, F. S., Fourcaud, N., & Abbott, L. F. (2001). Effects of synaptic noise and filtering on the frequency response of spiking neurons. *Physical Review Letters*, 86, 2186–2189.
- Chacron, M., Longtin, A., & Maler, L. (2000). Suprathreshold stochastic firing dynamics with memory in p-type electroreceptors. *Physical Review Letter*, 85, 1576–1579.
- Chacron, M., Pakdaman, K., & Longtin, A. (2003). Interspike interval correlations, memory, adaptation, and refractoriness in a leaky integrate-and-fire model with threshold fatigue. *Neural Computation*, 15, 253–278.
- Cox, D. R. (1962). *Renewal theory*. London: Methuen.

- Dayan, P., & Abbott, L. (2001). *Theoretical neuroscience: Computational and mathematical modeling of neural systems*. Cambridge, MA: MIT Press.
- Destexhe, A., Contreras, D., & Steriade, M. (1998). Mechanisms underlying the synchronizing action of corticothalamic feedback through inhibition of thalamic relay cells. *Journal of Neurophysiology*, *79*, 999–1016.
- Destexhe, A., Rudolph, M., Fellous, J., & Sejnowski, T. J. (2001). Fluctuating synaptic conductances recreate in vivo-like activity in neocortical neurons. *Neuroscience*, *107*, 13–24.
- Destexhe, A., Rudolph, M., & Paré, D. (2003). The high-conductance state of neocortical neurons in vivo. *Nature Reviews Neuroscience*, *4*, 739–751.
- Devroye, L. (1986). *Non-uniform random variate generation*. New York: Springer-Verlag.
- Diesmann, M., & Gewaltig, M.-O. (2002). NEST: An environment for neural systems simulations. In T. Plesser & V. Macho (Eds.), *Forschung und wissenschaftliches Rechnen, Beiträge zum Heinz-Billing-Preis 2001* (Vol. 58, pp. 43–70). Göttingen: Ges. für Wiss. Datenverarbeitung.
- Diesmann, M., Gewaltig, M.-O., & Aertsen, A. (1999). Stable propagation of synchronous spiking in cortical neural networks. *Nature*, *402*, 529–533.
- Ermentrout, B., Pascal, M., & Gutkin, B. (2001). The effects of spike frequency adaptation and negative feedback on the synchronization of neural oscillators. *Neural Computation*, *13*, 1285–1310.
- Fourcaud, N., & Brunel, N. (2002). Dynamics of the firing probability of noisy integrate-and-fire neurons. *Neural Computation*, *14*, 2057–2110.
- Fuhrmann, G., Markram, H., & Tsodyks, M. (2002). Spike frequency adaptation and neocortical rhythms. *Journal of Neurophysiology*, *88*, 761–770.
- Gardiner, C. W. (1984). Adiabatic elimination in stochastic systems. I. formulation of methods and application to few-variable systems. *Physical Review A*, *29*, 2814–2823.
- Gardiner, C. W. (1985). *Handbook of stochastic methods*. Berlin: Springer-Verlag.
- Gazères, N., Borg-Graham, L. J., & Frégnac, Y. (1998). A phenomenological model of visually evoked spike trains in cat geniculate nonlagged x-cells. *Visual Neuroscience*, *15*, 1157–1174.
- Gerstner, W. (1995). Time structure of the activity in neural network models. *Physical Review E*, *51*, 738–758.
- Gerstner, W. (2000). Population dynamics of spiking neurons: Fast transients, asynchronous states, and locking. *Neural Computation*, *12*, 43–89.
- Gerstner, W. (2001). Coding properties of spiking neurons: Reverse and cross-correlations. *Neural Networks*, *14*, 599–610.
- Gerstner, W., Kempter, R., van Hemmen, J. L., & Wagner, H. (1996). A neuronal learning rule for sub-millisecond temporal coding. *Nature*, *383*, 76–78.
- Gerstner, W., & Kistler, W. (2002). *Spiking neuron models: Single neurons, populations, plasticity*. Cambridge: Cambridge University Press.
- Haken, H. (1983). *Synergetics* (3rd ed.). Berlin: Springer-Verlag.
- Hines, M. L., & Carnevale, N. T. (1997). The NEURON simulation environment. *Neural Computation*, *9*, 1179–1209.
- Ihaka, R., & Gentleman, R. (1996). R: A language for data analysis and graphics. *Journal of Computational and Graphical Statistics*, *5*(3), 299–314.

- Knight, B. W. (1972). Dynamics of encoding in a population of neurons. *Journal of General Physiology*, *59*, 734–766.
- Knight, B. W. (2000). Dynamics of encoding in neuron populations: Some general mathematical features. *Neural Computation*, *12*, 473–518.
- Knight, B. W., Omurtag, A., & Sirovich, L. (2000). The approach of a neuron population firing rate to a new equilibrium: An exact theoretical result. *Neural Computation*, *12*, 1045–1055.
- Koch, C. (1999). *Biophysics of computation: Information processing in single neurons*. New York: Oxford University Press.
- La Camera, G., Rauch, A., Lüscher, H.-R., Senn, W., & Fusi, S. (2004). Minimal models of adapted neuronal response to in vivo-like input currents. *Neural Computation*, *16*, 2101–2124.
- Latham, P. E., Richmond, B. J., Nelson, P. G., & Nirenberg, S. (2000). Intrinsic dynamics in neuronal networks. I. theory. *Journal of Neurophysiology*, *83*, 808–827.
- Lindner, B., & Longtin, A. (2003). Nonrenewal spike trains generated by stochastic neuron models. In *SPIE Proceedings 5114 (Fluctuations and Noise)* (pp. 209–218). Bellingham, WA: SPIE.
- Longtin, A., & Racicot, D. (1997). Spike train patterning and forecastability. *Biosystems*, *40*, 111–118.
- Mainen, Z., & Sejnowski, T. J. (1995). Reliability of spike timing in neocortical neurons. *Science*, *268*, 1503–1505.
- McCormick, D., Connors, B., Lighthall, J., & Prince, D. (1985). Comparative electrophysiology of pyramidal and sparsely spiny stellate neurons of the neocortex. *Journal of Neurophysiology*, *54*, 782–806.
- Meffin, H., Burkitt, A. N., & Grayden, D. B. (2004). An analytical model for the “large, fluctuating synaptic conductance state” typical of neocortical neurons in-vivo. *Journal of Computational Neuroscience*, *16*, 159–175.
- Moreno-Bote, R., & Parga, N. (2004). Role of synaptic filtering on the firing response of simple model neurons. *Physical Review Letters*, *92*, 028102.
- Moreno-Bote, R., & Parga, N. (2005). Membrane potential and response properties of populations of cortical neurons in the high conductance state. *Physical Review Letters*, *94*, 088103.
- Muller, E. (2003). *Simulation of high-conductance states in cortical neural networks*. M.Sc. thesis, University of Heidelberg.
- Nawrot, M. P., Boucsein, C., Rodriguez-Molina, V., Aertsen, A., Grün, S., & Rotter, S. (2007). Serial interval statistics of spontaneous activity in cortical neurons in vivo and in vitro. *Neurocomputing*, *70*, 1717–1722.
- Nykamp, D. Q., & Tranchina, D. (2000). A population density approach that facilitates large-scale modeling of neural networks: Analysis and an application to orientation tuning. *Journal of Computational Neuroscience*, *8*, 51–63.
- Nykamp, D. Q., & Tranchina, D. (2001). A population density approach that facilitates large-scale modeling of neural networks: Extension to slow inhibitory synapses. *Neural Computation*, *13*, 511–546.
- O’Brien, B. J., Isayama, T., Richardson, R., & Berson, D. M. (2002). Intrinsic physiological properties of cat retinal ganglion cells. *Journal of Physiology*, *538*, 787–802.

- Omurtag, A., Knight, B. W., & Sirovich, L. (2000). On the simulation of large populations of neurons. *Journal of Computational Neuroscience*, 8, 51–63.
- Papoulis, A., & Pillai, S. U. (1991). *Probability, random variables and stochastic processes* (4th ed.). New York: McGraw-Hill.
- Renart, A., Brunel, N., & Wang, X.-J. (2004). Mean-field theory of irregularly spiking neuronal populations and working memory in recurrent cortical networks. In J. Feng (Ed.), *Computational neuroscience: A comprehensive approach* (pp. 431–490). New York: Chapman&Hall/CRC.
- Ricciardi, L. (1977). *Diffusion processes and related topics in biology*. Berlin: Springer-Verlag.
- Richardson, M. J. E. (2004). Effects of synaptic conductance on the voltage distribution and firing rate of spiking neurons. *Physical Review E*, 69(5), 051918.
- Richardson, M. J. E., & Gerstner, W. (2005). Synaptic shot noise and conductance fluctuations affect the membrane voltage with equal significance. *Neural Computation*, 17, 923–947.
- Rieke, F., Warland, D., de Ruyter van Steveninck, R., & Bialek, W. (1997). *Spikes: Exploring the neural code*. Cambridge, MA: MIT Press.
- Risken, H. (1996). *The Fokker-Planck equation: Methods of solution and applications* (2nd ed.). Berlin: Springer-Verlag.
- Rudolph, M., & Destexhe, A. (2003a). Characterization of subthreshold voltage fluctuations in neuronal membranes. *Neural Computation*, 15, 2577–2618.
- Rudolph, M., & Destexhe, A. (2003b). The discharge variability of neocortical neurons during high-conductance states. *Neuroscience*, 119, 885–873.
- Rudolph, M., & Destexhe, A. (2005). An extended analytic expression for the membrane potential distribution of conductance-based synaptic noise. *Neural Computation*, 17, 2301–2315.
- Shadlen, M., & Newsome, W. (1998). The variable discharge of cortical neurons: Implications for connectivity, computation, and information coding. *Journal of Neuroscience*, 18, 3870–3896.
- Shea, B. L. (1988). Algorithm AS 239, incomplete gamma function. *Applied Statistics*, 37, 466–473.
- Shelley, M., McLaughlin, D., Shapley, R., & Wielaard, D. (2002). States of high conductance in a large-scale model of the visual cortex. *Journal of Computational Neuroscience*, 13, 93–109.
- Siebert, A. J. F. (1951). On the first passage time probability function. *Physical Review*, 81, 617–623.
- Smith, G. D., Cox, C. L., Sherman, S. M., & Rinzel, J. (2001). A firing-rate model of spike-frequency adaptation in sinusoidally-driven thalamocortical relay neurons. *Thalamus and Related Systems*, 1, 135–156.
- Softky, W. R., & Koch, C. (1993). The highly irregular firing of cortical cells is inconsistent with temporal integration of random EPSPs. *Journal of Neuroscience*, 13, 334–350.
- Song, S., & Abbott, L. F. (2001). Cortical remapping through spike timing-dependent synaptic plasticity. *Neuron*, 32, 1–20.
- Song, S., Miller, K., & Abbott, L. F. (2000). Competitive Hebbian learning through spike-timing-dependent synaptic plasticity. *Nature Neuroscience*, 3, 919–926.

- van Rossum, M. C. W., Bi, G. Q., & Turrigiano, G. G. (2000). Stable Hebbian learning from spike timing-dependent synaptic plasticity. *Journal of Neuroscience*, *20*(23), 8812–8821.
- van Vreeswijk, C. A., & Hansel, D. (2001). Patterns of synchrony in neural networks with spike adaptation. *Neural Computation*, *13*, 959–992.
- Whittaker, E. T., & Robinson, G. (1967). *The calculus of observations: A treatise on numerical mathematics* (4th ed.). New York: Dover.
- Wilson, H. R., & Cowan, J. D. (1972). Excitatory and inhibitory interactions in localized populations of model neurons. *Biophysical Journal*, *12*, 1–24.

Received November 7, 2005; accepted February 15, 2007.

This article has been cited by:

1. Imke C.G. Reimer, Benjamin Staude, Werner Ehm, Stefan Rotter. 2012. Modeling and analyzing higher-order correlations in non-Poissonian spike trains. *Journal of Neuroscience Methods* **208**:1, 18-33. [[CrossRef](#)]
2. Martin Paul Nawrot. 2012. Dynamics of sensory processing in the dual olfactory pathway of the honeybee. *Apidologie* **43**:3, 269-291. [[CrossRef](#)]
3. Gabriel Koch Ocker, Thanos Tzounopoulos, Brent Doiron. 2012. Adaptation shapes spike train correlations: theory and application to tinnitus. *BMC Neuroscience* **13**:Suppl 1, P146. [[CrossRef](#)]
4. Eugenio Urdapilleta. 2011. Onset of negative interspike interval correlations in adapting neurons. *Physical Review E* **84**:4. . [[CrossRef](#)]
5. Moritz Deger, Moritz Helias, Clemens Boucsein, Stefan Rotter. 2011. Statistical properties of superimposed stationary spike trains. *Journal of Computational Neuroscience* . [[CrossRef](#)]
6. Farzad Farkhooi, Eilif Muller, Martin Nawrot. 2011. Adaptation reduces variability of the neuronal population code. *Physical Review E* **83**:5. . [[CrossRef](#)]
7. Felipe Gerhard, Robert Haslinger, Gordon Pipa. Applying the Multivariate Time-Rescaling Theorem to Neural Population Models. *Neural Computation*, ahead of print1-32. [[Abstract](#)] [[PDF](#)] [[PDF Plus](#)]
8. W. H. Nesse, L. Maler, A. Longtin. 2010. Biophysical information representation in temporally correlated spike trains. *Proceedings of the National Academy of Sciences* **107**:51, 21973-21978. [[CrossRef](#)]
9. A. Yu. Buchin, A. V. Chizhov. 2010. Firing-rate model of a population of adaptive neurons. *Biophysics* **55**:4, 592-599. [[CrossRef](#)]
10. Moritz Deger, Moritz Helias, Stefano Cardanobile, Fatihcan Atay, Stefan Rotter. 2010. Nonequilibrium dynamics of stochastic point processes with refractoriness. *Physical Review E* **82**:2. . [[CrossRef](#)]
11. Rubén Moreno-Bote, Néstor Parga. 2010. Response of Integrate-and-Fire Neurons to Noisy Inputs Filtered by Synapses with Arbitrary Timescales: Firing Rate and Correlations. *Neural Computation* **22**:6, 1528-1572. [[Abstract](#)] [[Full Text](#)] [[PDF](#)] [[PDF Plus](#)] [[Supplementary Content](#)]
12. Jens Kremkow, Laurent U. Perrinet, Guillaume S. Masson, Ad Aertsen. 2010. Functional consequences of correlated excitatory and inhibitory conductances in cortical networks. *Journal of Computational Neuroscience* **28**:3, 579-594. [[CrossRef](#)]
13. Stefano Cardanobile, Stefan Rotter. 2010. Multiplicatively interacting point processes and applications to neural modeling. *Journal of Computational Neuroscience* **28**:2, 267-284. [[CrossRef](#)]

14. Cheng Ly, G. Bard Ermentrout. 2010. Analysis of Recurrent Networks of Pulse-Coupled Noisy Neural Oscillators. *SIAM Journal on Applied Dynamical Systems* **9**:1, 113-137. [[CrossRef](#)]
15. Cheng Ly, Daniel Tranchina. 2009. Spike Train Statistics and Dynamics with Synaptic Input from any Renewal Process: A Population Density Approach. *Neural Computation* **21**:2, 360-396. [[Abstract](#)] [[Full Text](#)] [[PDF](#)] [[PDF Plus](#)]
16. Wiebke Potjans, Abigail Morrison, Markus Diesmann. 2009. A Spiking Neural Network Model of an Actor-Critic Learning Agent. *Neural Computation* **21**:2, 301-339. [[Abstract](#)] [[Full Text](#)] [[PDF](#)] [[PDF Plus](#)]
17. Farzad Farkhooi, Martin Strube-Bloss, Martin Nawrot. 2009. Serial correlation in neural spike trains: Experimental evidence, stochastic modeling, and single neuron variability. *Physical Review E* **79**:2. . [[CrossRef](#)]
18. Ibiyinka Fuwape, Alexander Neiman. 2008. Spontaneous firing statistics and information transfer in electroreceptors of paddlefish. *Physical Review E* **78**:5. . [[CrossRef](#)]
19. Giancarlo La Camera, Michele Giugliano, Walter Senn, Stefano Fusi. 2008. The response of cortical neurons to in vivo-like input current: theory and experiment. *Biological Cybernetics* **99**:4-5, 279-301. [[CrossRef](#)]
20. M DEKAMPS, V BAIER, J DREVER, M DIETZ, L MOSENLECHNER, F VANDERVELDE. 2008. The state of MIIND. *Neural Networks* **21**:8, 1164-1181. [[CrossRef](#)]
21. Z PIWKOWSKA, M POSPISCHIL, R BRETTE, J SLIWA, M RUDOLPHLILITH, T BAL, A DESTEXHE. 2008. Characterizing synaptic conductance fluctuations in cortical neurons and their influence on spike generation. *Journal of Neuroscience Methods* **169**:2, 302-322. [[CrossRef](#)]
22. Lars Wolff, Benjamin Lindner. 2008. Method to calculate the moments of the membrane voltage in a model neuron driven by multiplicative filtered shot noise. *Physical Review E* **77**:4. . [[CrossRef](#)]